Computers and Structures 322 (2026) 108120

Contents lists available at ScienceDirect

Computers and Structures

journal homepage: www.elsevier.com/locate/compstruc

Physics-Informed neural network based inversion and prediction of natural chloride diffusion in uncracked and cracked concrete systems☆

Zhewen Huang [a,*], Senlin Xie [a,b,*], Kasyapa Sriram Kompella [a], Estefanía Cuenca [a], Stefano Mariani [a], Liberato Ferrara [a]

[a] Department of Civil and Environmental Engineering, Politecnico di Milano, Piazza Leonardo da Vinci 32, 20133 Milan, Italy
[b] State Key Laboratory of Intelligent Geotechnics and Tunnelling, College of Civil and Transportation Engineering, Shenzhen University, Nanhai Avenue Nanshan District 3688, 518060 Shenzhen, China

ARTICLE INFO

Keywords:
Physics-informed neural network
Chloride diffusion
Inversion
Self-healing concrete
Fick 2nd law

ABSTRACT

Studying chloride diffusion in concrete is essential for predicting structural durability and designing corrosion-resistant materials and structures. While analytical models and finite element methods can simulate diffusion, they typically require large and high-quality datasets and do not possess advantages in parameter identification. Physics-Informed Neural Network, which integrates Fick 2nd law with initial and boundary conditions, offer a promising alternative. It not only replicates diffusion behavior accurately but also enhances the fitting of experimental data via a data-driven loss term and enable inverse estimation of diffusion related parameters. This paper outlines three key advantages of using this new method for problem-solving about chloride diffusion in concrete: (1) robustness to noise and low data requirements for one-dimensional inverse estimation of diffusion coefficients; (2) strategy integrates data, physics, and engineering insights for parameter inversion.; and (3) extended physics-informed frameworks with weak constraints for cracked concrete. Overall, Physics-Informed Neural Network provides a robust numerical tool for efficient durability assessment and the design of corrosion-resistant and resilient concrete structures. For self-healing concrete, the proposed framework effectively estimates diffusion coefficient in healed crack and accurately predicts long-term diffusion behavior, contributing to the optimal design and evaluation of self-healing materials.

1. Introduction

Concrete, a material widely employed in engineering and infrastructure construction, is frequently combined with steel reinforcement, resulting in reinforced concrete that is often subject to complex and increasingly severe service conditions. In marine environments corrosive ions, represented by chloride ions, upon reaching a critical concentration can activate corrosion, which, because of severe reduction of the bonding capacity of the steel reinforcement to the concrete and reduction of the steel resistant area, is likely to result into safety issues and serious economic losses [1,2]. Therefore, reliably predicting chloride ion diffusion in concrete is crucial for the durability design of new and the retrofit of existing damaged concrete structures.

Due to its nature, concrete can be approximated as a homogeneous and continuous porous medium on a macroscopic scale, enabling the application of Fick 2nd law to describe the spatial and temporal variation of chloride concentration upon a diffusion driven phenomenon. In particular, the error function solution based on this law is widely employed for field evaluations in practical engineering and is equally applicable in laboratory studies, owing to its simple mathematical formulation and strong potential for further development. Mathematical models from Life-365 [3], fib Model Code (2020) [4], and DuraCrete [5] have been developed using this error function solution. The ClinConc Model considers both the free and bound chloride in migration and describes the transition between the free and bound states of chloride ions in concrete using mass balance equations in combination with a nonlinear chloride binding isotherm [6]. This allows the predicted diffusive behavior to reflect the actual situation over time. Although incorporating multi-parameter models in these methods has theoretically enhanced the accuracy of describing chloride diffusion processes, significant challenges remain in practical applications. These include the high demand for experimental data and the reliance on extensive long-

☆ This article is part of a special issue entitled: 'CAS_ARTISTE25' published in Computers and Structures.

* Corresponding authors.
E-mail addresses: zhewen.huang@polimi.it (Z. Huang), xiesenlin@szu.edu.cn (S. Xie).

https://doi.org/10.1016/j.compstruc.2026.108120
Received 7 November 2025; Accepted 19 January 2026

term datasets for parameter identification and model calibration. Such requirements pose monetary challenges and are further complicated by issues related to data reproducibility and the diversity of field conditions, thereby limiting the model's generalizability and application scope.

Numerical simulations have thus become an efficient tool and are increasingly widely and intensively used in concrete design-oriented research, playing an important role especially in the prediction of durability performance. The finite element method (FEM), grounded in robust theoretical principles and advanced numerical techniques, effectively describes the macroscopic problem of chloride diffusion in concrete while flexibly handling complex boundary conditions and multi-field coupling challenges [7,8]. In contrast, the lattice discrete particle model (LDPM) offers the advantage of capturing inter-particle interactions, crack evolution, and localized damage phenomena within concrete, which is crucial for modeling local transport changes associated with crack propagation [9,10], more advantage of this method could be found in table 1. However, because LDPM accounts for numerous inter-particle interactions and fine-scale damage mechanisms, its numerical solution is computationally intensive, making it challenging to apply directly to long-term diffusion simulations in large-scale engineering structures. Moreover, both FEM and LDPM rely heavily on the accuracy of experimental data and material parameters. The sensitivity of parameters and the complexity of coupling effects further complicate the calibration and validation of these models in practical applications.

With the rapid advancement of artificial intelligence technologies, breakthroughs are increasingly being achieved in solving complex engineering problems that were traditionally considered intractable [11–14]. As an emerging method, the Physics-Informed Neural Network (PINN) has garnered widespread attention for addressing engineering challenges [15–17]. In the context of concrete chloride diffusion, although numerous machine learning and deep learning techniques have been applied [18], PINN offers several significant advantages: (1) Compared to traditional numerical simulation methods, it reduces the reliance on extensive datasets and can achieve higher prediction accuracy with limited data and computational resources. (2) Unlike purely data-driven methods, PINN integrates physical laws into the neural network training process, thereby providing reliable and continuous predictions rather than merely producing discrete, scattered data [14,19,20]. By merging data-driven approaches with physical priors, PINN achieves adaptive adjustment to complex boundary conditions (including time-varying ones) and parameter uncertainties, thus reducing the strict dependence of the model on experimental parameters [21]. (3) Although the FEM is generally more efficient than PINNs in terms of single-run computation time and resource usage, PINNs offer anther fundamental advantage in solving inverse problems. Specifically, a PINN can embed both the governing PDE constraints and the measurement observations directly into the loss function, enabling end-to-end simultaneous estimation of the field variables and unknown parameters without repeatedly solving the forward problem at each parameter update [22].

Despite its advantages, the application of the PINN model to chloride transport in concrete still faces several limitations: (1) Some studies have not fully integrated the data-driven component into the model, leading to overly idealized predictions [23,24]. (2) The time-varying nature of input parameters, such as surface concentration and diffusion coefficient, has often been neglected [25]. (3) The potential of PINN in solving inverse problems has not been fully leveraged within diffusion modeling; current applications typically estimate only a single diffusion coefficient [23,26,27], rather than addressing dual parameters related to diffusion. (4) More importantly the capability of PINN in solving two-dimensional diffusion problems (especially considering diffusion phenomena in the presence of cracks) has not been fully explored. When employing non-supervised PINN alone, the significant scale disparity between cracks and concrete, coupled with notable diffusion differences across the two domains, poses a coupled challenge. In addition, PINN can be used to solve the problem of chloride diffusion in concrete containing self-healing features. In the study of self-healing mechanisms in cracked concrete, measuring and estimating the diffusion coefficients of self-healing products faces multiple challenges due to the very small size of the cracks. Firstly, in the microscale environment, factors such as the pore structure, surface effects, and local temperature and humidity significantly affect the diffusion process, which makes it difficult to directly apply traditional macroscopic diffusion models. Secondly, self-healing products are often multi-component or multi-phase systems, and their complex physicochemical properties may lead to significant differences in their diffusion behaviors from those of ordinary substances, thus increasing the uncertainty of diffusion coefficient estimation. In addition, existing measurement techniques in the laboratory are often limited in resolution and sensitivity when dealing with such small scales, making it more difficult to obtain accurate data.

A summary of the pros and cons of each of the aforesaid approaches is provided in Table 1.

To address these issues and demonstrate the potential of the PINN model for studying chloride diffusion in concrete, this study proposes a framework that simultaneously tackles both forward and inverse problems. For the forward problem, the PINN model achieves performance comparable to that of the traditional FEM model in predicting concentration changes, while effectively incorporating actual experimental data through its data-driven component. For inverse problems, the PINN model effectively estimates key diffusion parameters by incorporating experimental data into the model through backpropagation. This approach demonstrates high accuracy, strong noise resistance, and a reduced need of large datasets. Furthermore, this study proposes an innovative application of the extended PINN model to simulate chloride transport within self-healing concrete, extending the one-dimensional diffusion model into a two-dimensional weakly supervised multiphase framework. The advantage of this approach lies in proposing a supervised extended PINN (xPINN) encompassing both the cementitious phase and the crack phase. Without requiring adaptive algorithmic optimization [28,29], it effectively resolves concentration disparities between phases caused by variations in diffusion coefficients and differences in diffusion domain dimensions. This is achieved simply by incorporating high-fidelity constraints at interfaces to obtain locally high-precision solutions, building upon the traditional xPINN framework [30,31]. Relying on the inverse problem-solving advantage of PINN itself, the diffusion coefficients of the healing products in the cracked phase are estimated. In conclusion, this study presents a simulation tool that integrates data-driven methodologies, physical constraints, and engineering expertise. Its reverse analysis capabilities provide significant support for AI design and assist in both engineering practice and laboratory research.

2. Theory and test of chloride diffusion

This section begins with the analytical solution derived from Fick 2nd law, followed by a description of the standard testing methods used to determine the chloride concentration distribution in concrete specimens.

2.1. Fick 2nd law and its error solution

The chloride concentration in concrete varies over time and is characterized by non-steady state diffusion. Generally, Fick 2nd law is widely used as the governing equation to describe the depth of penetration of chloride ions in concrete structures and its variation with time as follows:

$$\frac{\partial C(x,t)}{\partial t} = D\frac{\partial^2 C(x,t)}{\partial x^2} \tag{1}$$

Table 1
Methods on studying chloride diffusion in concrete.

Methodology	Advantage	Drawback
Analytical Method(1) Error Solution Based Models(2) ClinConc Model	(1) Fast and low computational cost(2) Suitable for theoretical research or preliminary estimation	(1) Requires large amounts of data to calibrate accurately(2) Cannot be easily extended to nonlinear or coupled problems
Finite Element Method 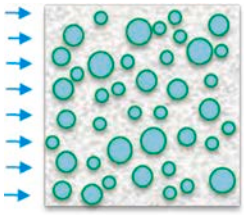	(1) Capable of handling complex geometries and boundary conditions(2) Good for performing multi-physics analyses	(1) Mesh generation and convergence(2) High computational cost
Lattice Discrete Particle Model 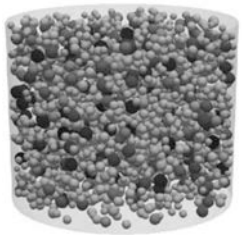	(1) Captures the heterogeneity of concrete at the mesoscale(2) Suitable for simulating cracks and local damage	(1) Complex modeling and high computational cost(2) Limited scalability to large structures
Physics-Informed Neural Network 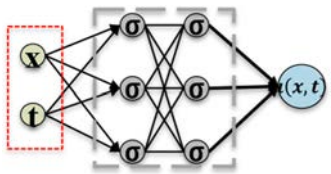	(1) Solves both **forward and inverse problems**(2) Integrates **real data and physical laws**(3) Potential for **2D problems** with irregular geometry	(1) High sensitivity to hyperparameters(2) High complexity and Low efficiency(3) Interpretability and reliability in training process

where $C(x,t)$ is total chloride concentration, and D represents the diffusion coefficient, which is affected by environmental factors or changes in material properties. x and t correspond to the distance of the test position from the concrete surface and the exposure time, respectively.

In saturated concrete, chloride transport satisfies the following assumptions: (1) the chloride concentration at the exposed surface is constant and given as c_s; (2) the chloride concentration inside the concrete is zero before the exposure starts; (3) a linear relationship exists between bound and free chloride; and (4) The diffusion behavior is modeled in a semi-infinite space. The error function solution to Fick 2nd law can be written as:

$$\frac{c(x,t)}{c_s} = 1 - erf\left(\frac{x}{2\sqrt{T}}\right) \tag{2}$$

where c represents the concentration of free chloride in the pore solution. In this case, the chloride is regarded as moving in a dilute solution and the parameter T can be defined as:

$$T = \int Ddt \tag{3}$$

If the chloride diffusion coefficient is constant, the parameter T in the classical error solution is:

$$T = D \bullet t \tag{4}$$

Numerous studies [32–35] have demonstrated that the chloride diffusion coefficient decreases with exposure time, particularly during the early stages when concrete exhibits a marked reduction in its diffusion coefficient because of aging. A number of studies have fitted the diffusion coefficient over time by means of a mathematical functional form (e.g., exponential [36]). The most classical and widely used of these is the Tang and Joost's expression for the diffusion coefficient over time, which introduced a reference diffusion coefficient D_{ref} and a reference age t_{ref}, and is given by the following expression [37]:

$$D(t_c) = D_{ref}\left(\frac{t_{ref}}{t_c}\right)^n \tag{5}$$

where t_c represents the concrete age; D_{ref} is the diffusion coefficient corresponding to the time t_{ref} (=7 or 28 days), and n is age factor, which ranges between 0 and 1. The above formula has been widely employed [3,4,38].

By substituting Eq. (5) into (3), the parameter T can be redefined as:

$$T = \int_{t_{ex}}^{t+t_{ex}} D(t_c)dt_c = \frac{D_{ref}}{1-n} \bullet \left[\left(1+\frac{t_{ex}}{t}\right)^{1-n} - \left(\frac{t_{ex}}{t}\right)^{1-n}\right] \bullet \left(\frac{t_{ref}}{t}\right)^n \bullet t \tag{6}$$

where t_{ex} is defined as the age of concrete at the start of exposure. With Eq. (6) known, the parameter T in Eq. (2) can be rewritten as:

$$T = \mathrm{D}_a \bullet t \tag{7}$$

in which:

$$D_a = \frac{D_{ref}}{1-n} \bullet \left[\left(1+\frac{t_{ex}}{t}\right)^{1-n} - \left(\frac{t_{ex}}{t}\right)^{1-n}\right] \bullet \left(\frac{t_{ref}}{t}\right)^n = D_{ref} \bullet \frac{f(t_{ex})}{1-n} \bullet \left(\frac{t_{ref}}{t}\right)^n \tag{8}$$

In general, D_a is commonly referred to as the apparent chloride diffusion coefficient. Under the assumption (3) or chloride binding is time-independent, the total chloride content, C, and surface concentration, C_s, expressed as a percentage by mass of concrete or cement, can be used as a replacement for c and c_s in the pore solution [35,37]. Therefore,

both Eqs. (4) and (7) can be expressed using the simplest model for chloride invasion in concrete:

$$\frac{C(x,t)}{C_s} = 1 - erf\left(\frac{x}{2\sqrt{\beta \bullet t}}\right) \tag{9}$$

where β could represent D when diffusion coefficient is assumed as a constant value. If time-variance needs to be considered, apparent diffusion coefficient D_a could be input into the above Eq. (9).

The error solutions discussed above are obtained under the condition that the surface concentration is constant, i.e., assumption (1). In addition, the time-varying nature of the surface concentration has been observed by many researchers, and the equations for the surface concentration as a function of time are summarized in Table 2. Except for the constant form, several functional forms can be used at an early stage to provide an initial fit or a quick estimate of the trend in the surface concentration of chloride ions over time. However, when considering long-term exposure, over decades, and a relatively stable external environment, the square root, power exponential and logarithmic forms do not have saturation values, i.e., the predicted surface concentration increases indefinitely over time. Especially in laboratory studies, where surface chloride concentrations tend to reach saturation values (C_0) in a relatively short period of time, an index function better describes this saturation process. In addition, Table 2 also lists the recommended fitting techniques, chosen according to the mathematical properties of the functions. Except for the index form, parameters for the other three expressions can be obtained by ordinary least-squares (OLS) fitting (or appropriate linearized variants). The index function is nonlinear because its parameters appear inside an exponential term, which precludes direct linear regression. Therefore, model parameters for that form were estimated by nonlinear least-squares fitting using the Levenberg–Marquardt algorithm.

2.2. Experiment on chloride concentration

To investigate the natural diffusion of chloride in the laboratory, an immersion test is typically conducted. In this test, the chloride concentration is measured at various depths after a specified immersion period, and regression analysis based on Eq. (9) is used to determine the diffusion coefficient and surface chloride concentrations (see Fig. 1). Natural chloride diffusion is slow in the absence of an applied electric field, and testing protocols differ slightly among various standards. For example, ASTM C1556 suggests immersing test specimens in a high-concentration sodium chloride solution (165 g/L) for at least 35 days to simulate long-term exposure in heavily chlorinated environments. EN12390-11 recommends immersing specimens in a 3% NaCl solution for at least 90 days, being a protocol designed to assess the long-term resistance of concrete to chloride exposure, particularly in marine structures. Transitioning from experimental measurements to simulation, it is worth highlighting that the measured surface chloride content can be anomalously low (e.g., see Fig. 1). This anomaly may result from factors such as mold contact, aggregate segregation, or dielectric interactions between the concrete surface and the chloride ion environment [32,39]. Therefore, direct measurement of surface chloride content may be unreliable, and the top layer of concrete is often discarded in experiments. A more robust approach involves fitting the chloride distribution curve, with surface chloride concentration and the diffusion coefficient treated as independent variables[36,40].

Table 2
Time-dependent mathematics models of..C_s

Functional form of C_s	Mathematics Model	Fitting technique	Reference
Constant	$C_s = C_0$	–	[58–60]
Square root	$C_s = k_0 + k_1 \bullet \sqrt{t}$	OLS	[35,58,61]
Index	$C_s = k_2 \bullet \left(1 - e^{-k_3 \bullet t}\right)$	Nonlinear Least Squares	[23,36,62,63]
Power exponent	$C_s = k_4 \bullet t^{k_5}$	Log–linear OLS	[61,64]
Logarithm	$C_s = k_6 \bullet ln(t) + k_7$	OLS	[50,58,65,66]

Note: k_i is the parameter obtained by the fitting technique.

3. Physics-informed neural network

Section 3 outlines the construction of the PINN model, including the network architecture and the physics- and data-based loss terms that underpin both forward prediction and inverse parameter identification.

3.1. General framework

In order to solve the complex modelling problem of the natural diffusion of chloride in concrete, a general computational framework based on PINNs is proposed in this paper. The core design of the framework (see Fig. 2) is outlined as follows: (1) Diffusion-related variables, specifically position and time, are randomly sampled and provided as inputs to a multilayer feed-forward neural network, which efficiently fits the chloride concentration field to capture the diffusion dynamics. (2) To enforce the classical physical law of diffusion, a physics-based loss term is incorporated into the model. This loss term comprises contributions from the initial conditions, boundary conditions (Dirichlet or Neumann), and the governing physical equation (Fick 2nd law). Additionally, the model can be configured to combine both physics-based and data-driven losses. (3) Partial derivatives required for computing the physical losses are obtained through automatic differentiation. (4) Optimization algorithms are employed to iteratively adjust the network parameters (weights and biases), ultimately leading to convergence of the loss function.

3.2. Deep neural network

A Deep Neural Network (DNN) consists of input layers, multiple hidden layers and output layers. Each layer consists of multiple neurons which are connected to each other by weights. The data enters from the input layer and passes through the nonlinear transformations of the layers, thus assisting the neuron output.

The study of chloride diffusion in concrete can usually be considered as a one-dimensional problem, with two variables, depth x and time t, in the input layer, and concentration in the output layer, a function approximator $\mathscr{H}$ can be constructed through the DNN:

$$u(x,t) \approx H(x,t,\theta) \tag{10}$$

where θ represents the parameters in neutral network, mainly including weight and bias.

The input layer receives two variables:

$$\mathrm{a}^{(0)} = \begin{bmatrix} x \\ t \end{bmatrix} \tag{11}$$

Assuming that there is a total of L layers between the input and output layers, the operations at each layer can be described as a single affine transformation (linear combination) plus the action of a nonlinear activation function. For instance, at the l^{th} layer ($l = 1, 2, 3, \cdots, L$), the computational processes are the following:

$$\mathrm{a}^{(l)} = \sigma^{(l)}\left[\mathrm{z}^{(l)}\right] = \sigma^{(l)}\left[\mathrm{W}^{(l)}\mathrm{a}^{(l-1)} + \mathrm{b}^{(l)}\right] \tag{12}$$

where $\mathrm{W}^{(l)}$ is the weight matrix for the l^{th} layer, which determines the effect of each neuron in the previous layer on the neurons in the current layer. $\mathrm{b}^{(l)}$ is the bias vector, which is response for the input to the

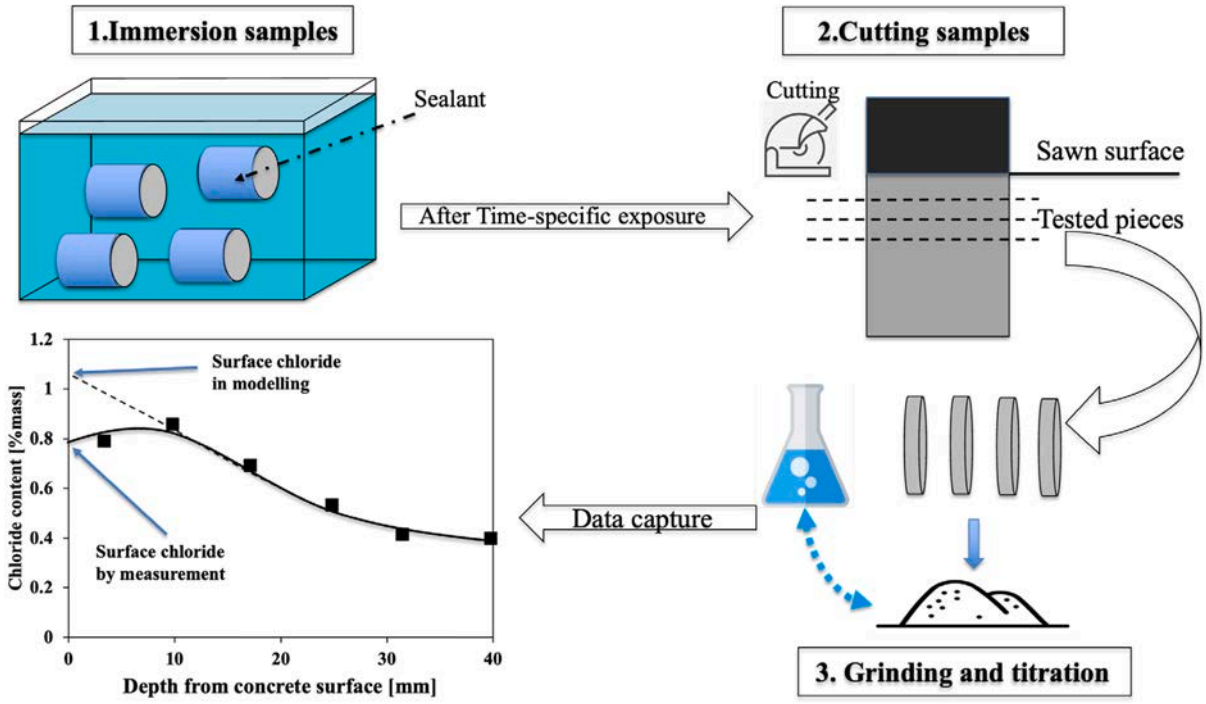

Fig. 1. Concentration test procedure in lab and estimation of diffusion parameters for chlorides.

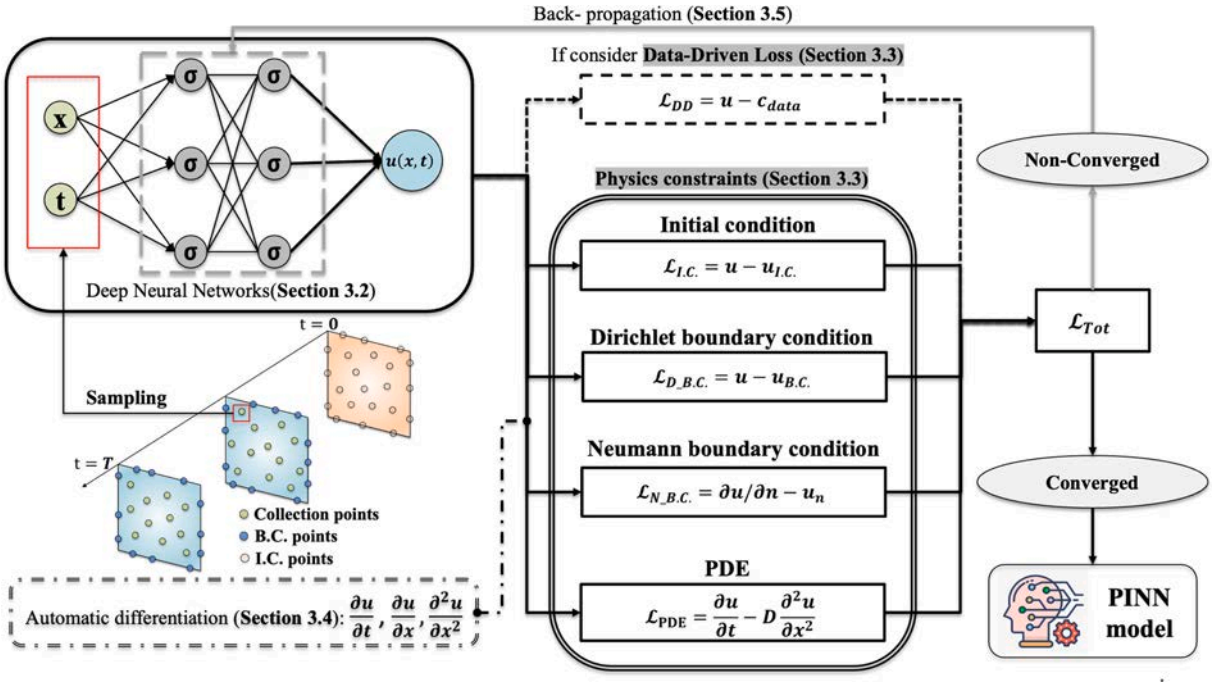

Fig. 2. The overall framework of PINN for solving chloride diffusion problems based on Fick 2nd law.

activation function. $\sigma^{(l)}$ is activation function applied componentwise used in this layer.

The diffusion problem based on Fick 2nd law mainly involves the calculation of the parameter gradient, and the solution of the diffusion equation is smooth and continuous. In this paper, the Tanh (hyperbolic tangent) function is chosen as the activation function of the neural network. The advantage of Tanh is that the function itself is a smooth and continuous nonlinear function, which is able to better approximate this kind of smoothly varying physical process [41,42]. This helps the network to more accurately capture the subtle trend of the concentration change with depth and time. Moreover, in order to guarantee output value u to be positive and in the range [0,1], sigmoid is therefore chosen as the activation function for the output layer.

3.3. Loss function and normalization

DNNs are widely used as a robust technique for dealing with classification and regression problems. As a data-driven approach, neural networks usually must minimize the difference between the actual

values (experimental results or observations) and the network's predicted values as a training goal. The mean square error (MSE) is usually adopted as the loss function for neural network training, as given below:

$$\mathscr{L}_{DD} = MSE_{DD} = \frac{1}{N_d}\sum_{j=1}^{N_d}\left(u_j(x_j,t_j) - c_j\right)^2 \tag{13}$$

where c_j is the actual values at position x_j and time t_j; N_d indicates the number of data points; and u_j represents the prediction from neural networks.

From the above, it can be observed that performing pure DNN training to achieve accurate convergence for prediction purposes, requires a large amount of training data to ensure the reliability of the network's operation, since there is no implicit guidance on the physics involved in the training of neural networks. The advantage of PINN lies in the introduction of physically informative constraints into the loss function, in order to achieve a reduction in the dependence on data and to guarantee the fulfilment of the corresponding physical laws. As the diffusion satisfies the partial differential equation (PDE) in Eq. (1), its governing loss function can be written as follows:

$$\mathscr{L}_{PDE} = MSE_{PDE} = \frac{1}{N}\sum_{k=1}^{N}\left(\frac{\partial u_k(x_k,t_k)}{\partial t} - D\frac{\partial^2 u_k(x_k,t_k)}{\partial x^2}\right)^2 \tag{14}$$

where a set of sampling points $\{(x_k,t_k)\}_{k=1}^{N}$ were selected.

In addition, the losses of the boundary conditions (B.C.) and initial conditions (I.C.) need to be also taken into account by randomly selecting a set of sampling points $\{(x_b,t_b)\}_{b=1}^{N_b}$ from the boundary and a set of sampling points $\{(x_i)\}_{i=1}^{N_i}$ at time $t = 0$. The corresponding loss function components can be written, respectively:

$$\mathscr{L}_{B.C.} = MSE_{B.C.} = \frac{1}{N_b}\sum_{b=1}^{N_b}\left(u_b(x_b,t_b) - c_b\right)^2 \tag{15}$$

$$\mathscr{L}_{I.C.} = MSE_{I.C.} = \frac{1}{N_i}\sum_{i=1}^{N_i}\left(u_i(x_i,t_i) - c_i\right)^2 \tag{16}$$

where c_b represents prescribed boundary values, which includes concentrations on the surface and far away from the surface, and c_i (assuming equal to 0) is concentration before water exposure.

After defining the necessary loss functions, it is crucial to address the challenge posed by data exhibiting different orders of magnitude, which can significantly affect model performance. Pre-normalizing the input variables not only accelerates convergence and enhances model robustness but also mitigates inter-metric effects and facilitates uniform weight updates during training. This thereby improves the performance of the optimization algorithm. Moreover, various normalization methods exist, and the choice should be tailored to the specific requirements of the machine learning model and its application [17,43]. In this paper, the simplest method of normalization (Min-Max normalization) is used to scale down the data to [0,1]. The process is the following:

$$x = L\hat{x}, t = T\hat{t}, u = U\hat{u} \tag{17}$$

where x and t are again the depth and exposure time from the sampling point of the actual data. In a data-driven method assisted framework, u represents the actual concentration; $\hat{x}$, $\hat{t}$ and $\hat{u}$ are the scaled depth, time and concentration coordinates; L, T and U are the normalization coefficients.

As the input quantities become dimensionless values after normalization, the inverse chain rule needs to be followed in the calculation of the loss function to reduce the physical significance of the individual loss components. In particular, the loss in the PDE part, which involves the partial differential calculation needs to be transformed as follows:

$$\begin{cases} \dfrac{\partial u}{\partial t} = \dfrac{U}{T}\dfrac{\partial \hat{u}}{\partial \hat{t}} \\ \dfrac{\partial u}{\partial x} = \dfrac{U}{L}\dfrac{\partial \hat{u}}{\partial \hat{x}} \\ \dfrac{\partial^2 u}{\partial x^2} = \dfrac{U}{L^2}\dfrac{\partial^2 \hat{u}}{\partial \hat{x}^2} \end{cases} \tag{18}$$

Ultimately the PDE portion of the loss can be rewritten as:

$$\frac{\partial u}{\partial t} - D\frac{\partial^2 u}{\partial x^2} = \frac{U}{T}\frac{\partial \hat{u}}{\partial \hat{t}} - D\frac{U}{L^2}\frac{\partial^2 \hat{u}}{\partial \hat{x}^2} \tag{19}$$

3.4. Automatic differentiation

Neural network operations typically employ three primary methods for calculating derivatives: automatic differentiation (AD), numerical differentiation (ND), and symbolic differentiation (SD). Compared to ND and SD, AD avoids issues related to expression expansion and computes gradients both accurately and efficiently. This advantage stems from AD use of the chain rule to decompose complex functions into a sequence of elementary operations [16,44]. Within the PINN framework, AD automatically computes the partial derivatives of the network output with respect to the input variables, that are the spatial and temporal dimensions. These variables are used to construct residual functions describing the physical laws, such as the residuals of the PDEs of Fick 2nd law, as well as the constraint terms of the boundary and initial conditions.

3.5. Back-propagation and network adjustment

In Eq. (3), it has been proposed that the neural network is an approximator, and each term has a contribution to the output of the network that is highly correlated with the input values, in addition to relying on the underlying parameters θ of the neural network (including bias and weights). It also relies on the network output variable u in each loss. All the loss terms can be summed up to get the overall loss, which is used as a comprehensive assessment metric for the overall performance of the model, as given by:

$$\mathscr{L}_{Tot.}(\theta) = \omega_{PDE}\bullet\mathscr{L}_{PDE}(\theta) + \omega_{B.C.}\bullet\mathscr{L}_{B.C.}(\theta) + \omega_{I.C.}\bullet\mathscr{L}_{I.C.}(\theta) + \omega_{data}\bullet\mathscr{L}_{DD}(\theta) \tag{20}$$

where ω_{PDE}, $\omega_{B.C.}$, $\omega_{I.C.}$, and ω_{data} represent the weights of the loss terms. In general, weighting of the terms is controlled to emphasize the focus of the model's study.

Finally, the optimal parameters are found by continuously adjusting the weights and biases in the feedforward neural network, using optimization algorithms to minimize the total loss function. It is also important to note that the hyperparameters in the neural network (including the learning rate, the number of hidden layers, the number of neurons per layer, etc.) need to be determined through tuning, to ensure the robustness of the model operation and performance.

3.6. Forward problem & inverse problem

Based on the working principles of the PINN described above, the proposed model can be applied to address the problem of natural chloride diffusion, as illustrated in Fig. 3. When the relevant physical information is known, the chloride diffusion process can be simulated using empirical formulae for the surface chloride concentration and diffusion coefficient of concrete (following Fick 2nd law), even without incorporating experimental data, it is referred to as a pure PINN (P-PINN) or a data-free PINN. Although FE simulations can model this process applied to similar conditions, the unique advantage of the PINN approach lies in its ability to integrate actual data constraints into the

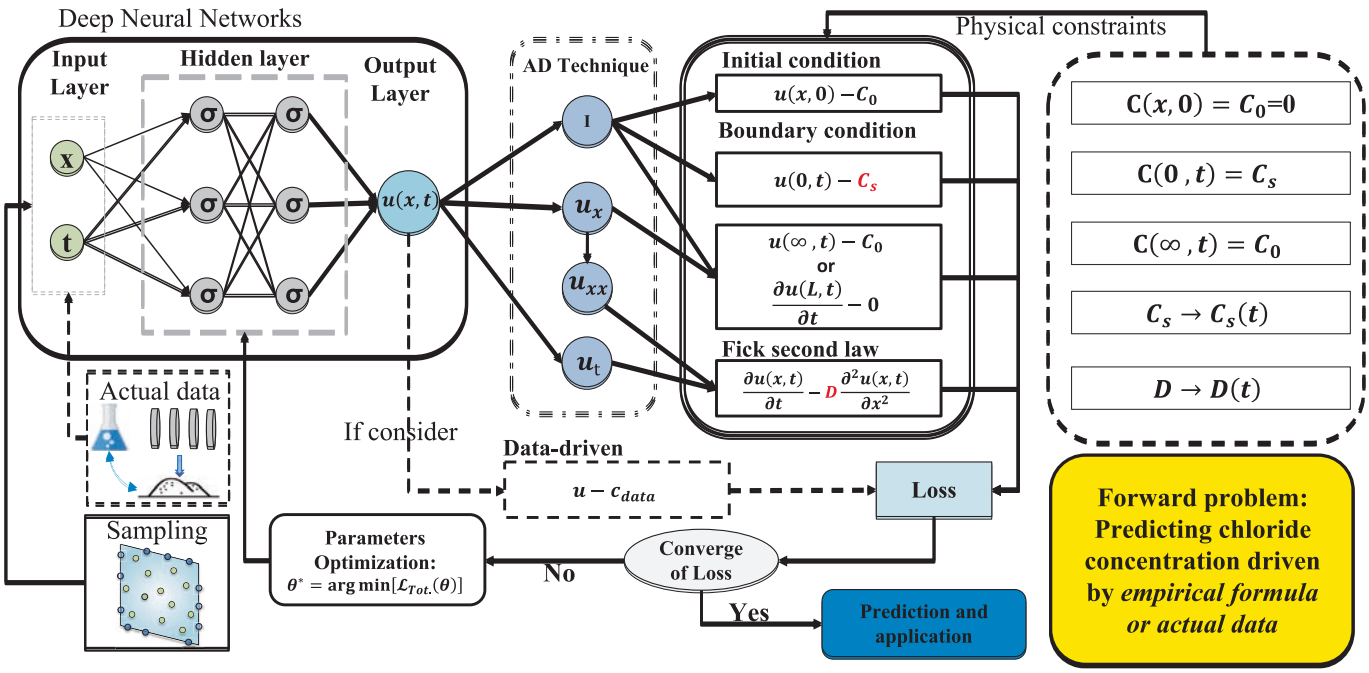

Fig. 3. PINN framework used for solving chloride concentration prediction.

calculations, hereinafter referred to as a data-driven PINN (DD-PINN). In this framework, Eq. (10) is fully embedded within the DNN to globally optimize the parameter θ^*, and the resulting expression is given by:

$$\theta^* = \text{argmin}[\mathscr{L}_{Tot.}(\theta)] \tag{21}$$

Beyond solving the forward problem with known material parameters and boundary conditions, the PINN framework can also perform inverse analysis by incorporating experimental concentration profiles into the loss function to identify the unknown diffusion parameters (β), as illustrated in Fig. 4. Guided by both data and physical constraints, the PINN network structure and the parameters within its iterative loss function are continuously updated, ultimately yielding the global optimal values or distributions for the diffusion coefficient D and the parameter θ. The global optimal solution can be expressed as:

$$\theta^*, \beta^* = \text{argmin}[\mathscr{L}_{Tot.}(\theta, \beta)] \tag{22}$$

4. Discussion on engineering applications of PINN

Section 4 then applies this framework to three case studies: uncracked concrete (one-dimensional), and cracked and self-healing concrete (two-dimensional), all following the same model construction, training and validation workflow unless stated otherwise.

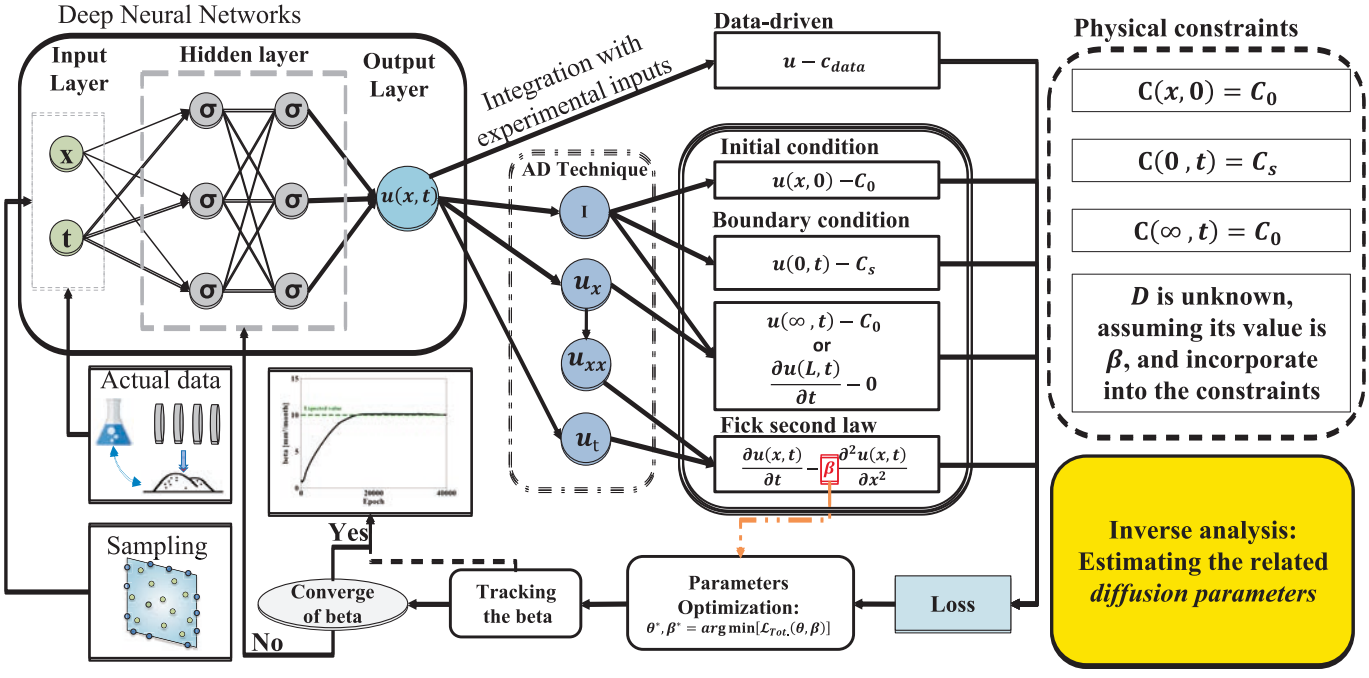

Fig. 4. PINN framework used for estimating related diffusion parameters.

4.1. Forward problem: Prediction of chloride transportation

To demonstrate the application of PINN in solving the forward problem of chloride transport in concrete, key physical parameters, including the surface chloride concentration and diffusion coefficient, must be determined prior to initiating neural network computations (See Appendix A). The time-varying function summarized by Cai et al [36] using the data presented in Fig. 5, was introduced into the PINN model for chloride diffusion studies. The specific functions are given by:

$$\begin{cases} C_s(t) = 1.056 \bullet \left(1 - e^{-0.24 \bullet t}\right) \\ D_a(t) = 21.92 \bullet e^{-0.126 \bullet t} \end{cases} \tag{23}$$

where the units of t and D_a are month and mm^2/month. In addition, data before Depth of 4 mm (convective zone) has been deleted, due to the reason introduced in Section 2.2.

Prior to employing the PINN method to simulate chloride ion diffusion in concrete, a classical finite element simulation of this process was conducted using COMSOL 6.2 software. This was undertaken to enable a systematic comparison of the performance of both methodologies [45]. The initial conditions of the relevant study, as well as the boundary conditions, are provided according to Fig. 6, which applies to both the modelling approaches. Fig. 6 shows a one-dimensional semi-infinite model for practical engineering studies; however, it is impossible to achieve true semi-infinity in the model. Therefore, careful consideration must be given to the boundary conditions at the far end. If the chloride concentration at the far boundary is equal to zero or initial values inside the concrete implies that chloride does not accumulate at that deep location over time, particularly when depth of concrete is sufficiently large. In general, given a finite field $0 \le x \le L$ in the model, L represents the distance from surface to far end. The value selection of L is critical, as it directly determines whether diffusion reaches the most distant boundary within the study timeframe. Guo et al [23]. have examined this problem in detail and found that a setting of 200 mm yields the optimal model performance in their study. In the laboratory experiments, concrete specimens are often coated on all, but one sides with a water-proofing material (see Fig. 1), leaving only one side in contact with the liquid, creating a unidirectional flow into the matrix and, in the absence of cracks, this diffusion can be considered a simple one-dimensional problem. At the far boundary, concentration gradient is considered zero due to the presence of the sealant.

Fig. 7 shows the random sampling of the PDE, initial condition and boundary condition with 3000, 1000 & 2000 collection points

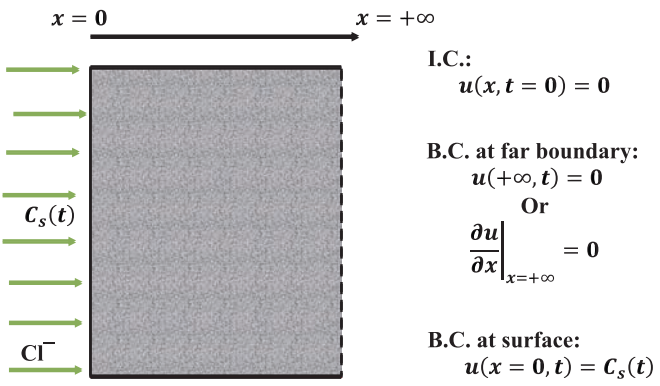

Fig. 6. Initial condition and Boundary conditions for 1D Diffusion.

respectively, and this sampling strategy is used in the following studies. Also included is a scatter of triangles, all of which are the experimental data points involved in Fig. 5. According to the operational architecture of the PINN in Fig. 3, a data-driven part could be added by including these data points in the model as well. It is emphasized that for a fairer comparison of finite element model versus the DD-PINN model, not all data points in Fig. 5 should be incorporated as a data-driven component into the DD-PINN. Therefore, these data points will be divided into two groups: one group (within the box in Fig. 5) will be integrated into the DD-PINN model, while the other group will be used to validate the difference in predictive performance between the PINN model and the finite element model on an unknown actual dataset. In addition, the information of some hyperparameters during this PINN training is shown in Table 3, more hyperparameters details in this diffusion problem could be referred by Shaban et al [26].

Fig. 8 compares the loss function evolution characteristics of P-PINN and DD-PINN during training. For P-PINN (Fig. 8(a)), due to the absence of a data-driven component, the total loss ultimately converges to an extremely low value, approaching 10^{-6}. At this stage, the model's performance was already satisfactory. By extending the training of iterations, a favorable convergence was eventually achieved, though this had a minor impact on the model's predictive performance. This indicates that without data constraints, the model effectively satisfies the control requirements of the partial differential equation, achieving a high level of physical consistency. In contrast, for DD-PINN (Fig. 8(b)), the loss variation is jointly driven by the PDE loss and the data-driven loss.

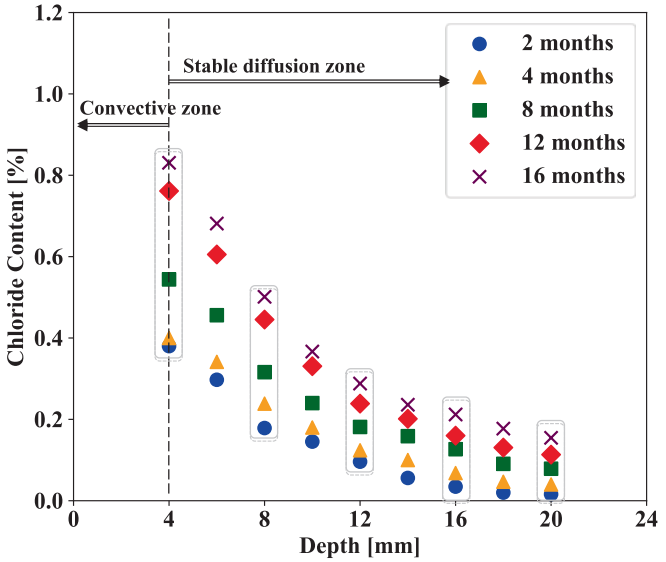

Fig. 5. Test data from Wang et al. (modified) [58].

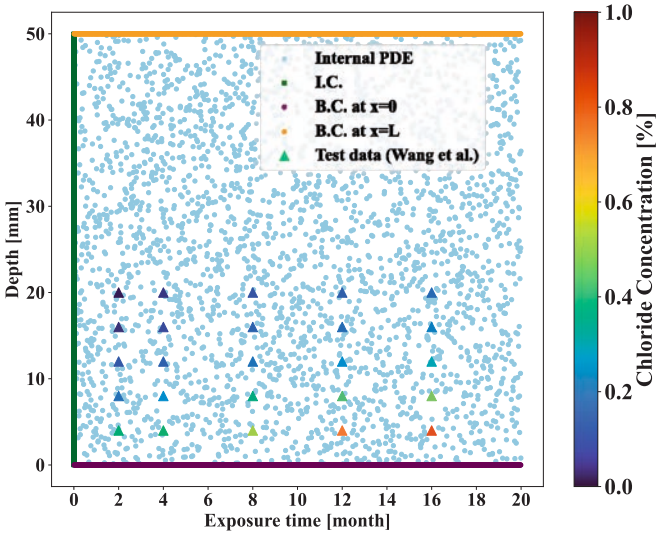

Fig. 7. Experimental data (within box line of Fig. 5) from Wang et al [58]. and sampling for PDE, I.C. and B.C.s in the PINN.

Table 3
General setting of the hyperparameters in neural network.

Hyperparameters	Value
Learning rate	0.001
Hidden layers	4
Neuron	32
Weight for I.C.	1
Weight for B.C.	1
Weight for PDE	1
Weight for data	1

During early training, the data-driven loss primarily drives the decrease in total loss. In the mid-to-late stages, while the PDE loss continues to decrease, the data-driven loss forms a lower bound on the error, causing the total loss to eventually stabilize at approximately 10^{-4}. This phenomenon indicates that when experimental data contains noise or measurement errors, the model cannot infinitely approach zero loss but instead reaches an achievable upper limit of accuracy determined by the data quality.

The numerical simulation results from COMSOL closely match those obtained from the P-PINN simulations, as illustrated in Figs. 9(a) and 9(b). Fig. 10(a) presents the predicted performance of both models after a specific exposure period. The near-overlap of the dashed and solid lines indicates that PINN can yield results comparable to traditional numerical simulation methods for the chloride diffusion problem, under the given conditions. A key advantage of this machine learning approach is its ability to directly incorporate experimental data into the simulation process through a loss term, resulting in outcomes that closely reflect real engineering conditions. This advantage is demonstrated in Fig. 9(c), where experimental data are used to calibrate the model while maintaining an overall diffusion trend that is consistent with the results from both P-PINN and COMSOL. This is particularly evident in Fig. 10(b), where the DD-PINN predictions align more closely with the actual chloride variation with depth compared to the early exposure predictions shown in Fig. 10(a). This discrepancy is quantified in Table 4 through comparison of three metrics: root mean square error (RMSE), mean absolute error (MAE), and determination coefficient (R^2). During the initial exposure period (2 months), COMSOL exhibited significantly larger prediction errors, with RMSE and MAE values of 0.1042 and 0.0838 respectively, significantly higher than DD-PINN's 0.0257 and 0.0176. Meanwhile, COMSOL's R2 was only 0.0527, barely capturing the experimental data trends, whereas DD-PINN achieved an R2 of 0.9423, demonstrating stable and reliable fitting capability even in the early stage. As exposure time increased (6–16 months), COMSOL's accuracy did gradually improve. However, its RMSE, MAE, and R2 consistently lagged DD-PINN, indicating persistent discrepancies in experimental agreement. In terms of overall dataset, DD-PINN achieved lower global errors (RMSE = 0.0133, MAE = 0.0114) and higher goodness-of-fit (R2 = 0.9953), significantly outperforming COMSOL (RMSE = 0.0504, MAE = 0.0433, R2 = 0.9332). Thus, the DD-PINN simulation not only adheres to the constraints imposed by physical laws but also aligns well with actual engineering outcomes.

4.2. *Inverse problem: Estimating diffusion related parameters*

4.2.1. *Estimating the single diffusion coefficient*

Based on the model framework illustrated in Fig. 4, the PINN model possesses the unique capability to solve inverse problems. To verify the feasibility and accuracy of the PINN model for inverse problem-solving, actual data must be incorporated into the estimation process. To prevent leakage of true parameter values into training, the diffusion coefficients used to generate synthetic concentrations were withheld from the training labels and from hyperparameter selection. Synthetic data were produced by an empirical forward model (Eq. (4)) using preset diffusion coefficients, ensuring consistency with Fick 2nd law. Experimentally measured diffusion coefficients are often affected by measurement error and sample-preparation variability and therefore are unsuitable as an absolute benchmark for inversion accuracy. Accordingly, the inversion capability of PINN was first validated on physically consistent synthetic data. The model was then transferred and validated on independent experimental data to assess its applicability and robustness under real measurement conditions.

To verify the feasibility and accuracy of the PINN model for estimating the single diffusion coefficient, the aforementioned synthetic data was generated by Fig. 11(a). Assuming a diffusion coefficient of $D = 10\text{mm}^2/\text{month}$ and considering various positions (depth = x) and exposure times t (see Fig. 11(b) for details), the generator computes the corresponding true concentrations $C_{real,training}$ (100 data points in total) using the classical empirical error function solution. This is then utilized in the loss term calculation for the data-driven component. Furthermore, it is important to clarify that during the model computation, only the depth x, time t, and generated concentrations are input into the PINN; the diffusion coefficient D which is used for data generation is not directly incorporated into the network operations. Therefore, the D is an unknown parameter for the PINN. In this inversion training network, the weight of the PDE needs to be increased (in general, 10 to 1000) to allow the network to value the loss of the PDE more highly, and thus more

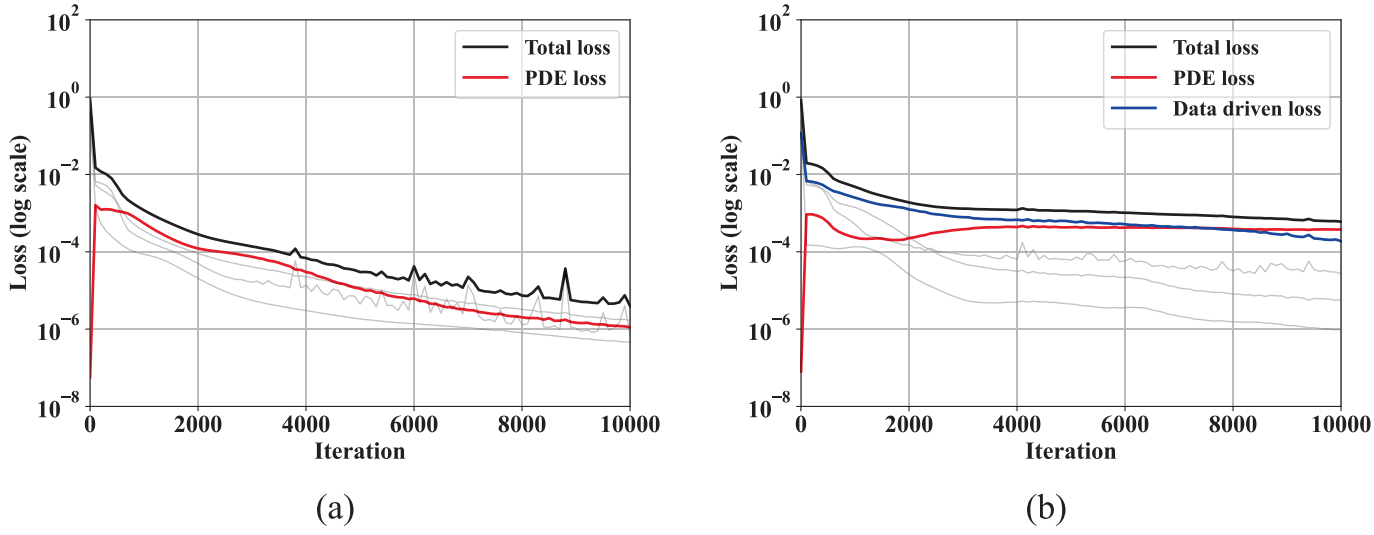

Fig. 8. The training loss of (a) P-PINN and (b) DD-PINN.

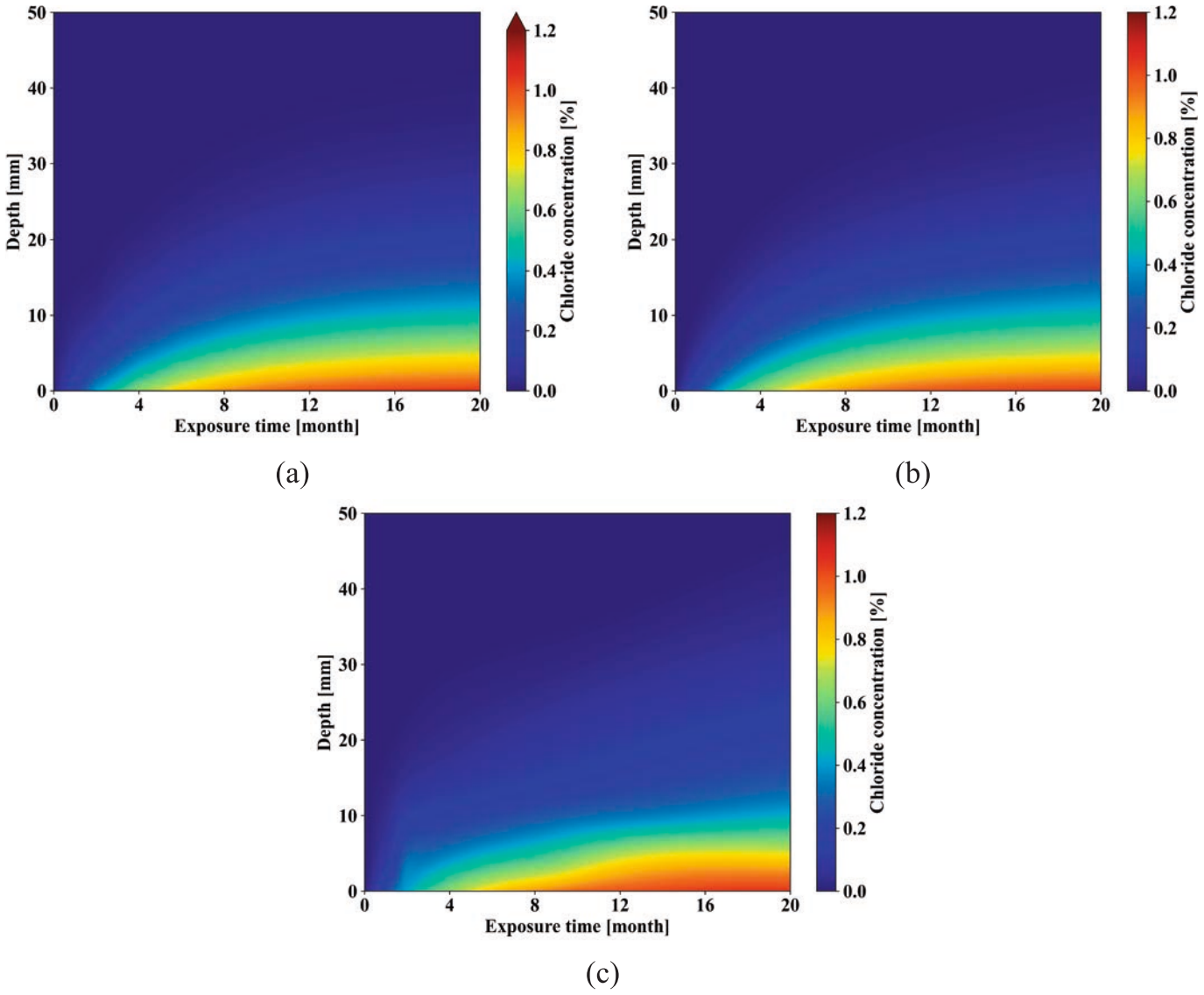

Fig. 9. Chloride concentration contour results of (a) COMSOL, (b) P-PINN and (c) DD-PINN.

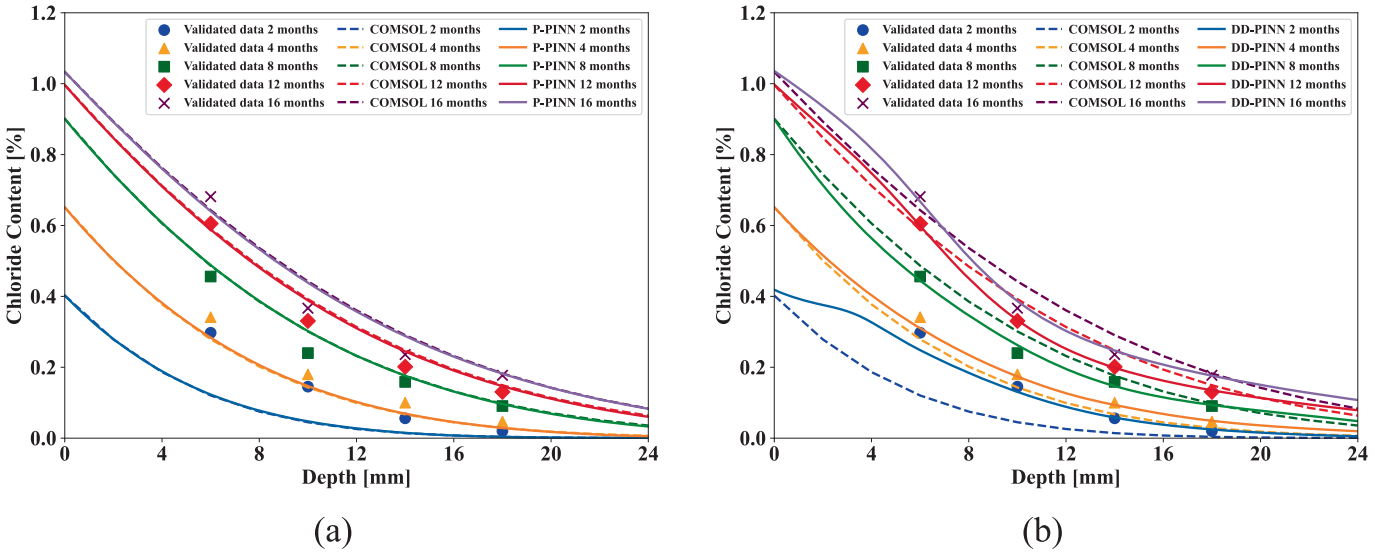

Fig. 10. Test results and COMSOL results, comparison with (a) P-PINN and (b) DD-PINN.

Table 4
Error indicators for DD-PINN and COMSOL results.

Exposure months	RMSE		MAE		R^2	
	COMSOL	DD-PINN	COMSOL	DD-PINN	COMSOL	DD-PINN
2 months	0.1042	0.0257	0.0838	0.0176	0.0527	0.9423
6 months	0.0408	0.0162	0.0375	0.0114	0.8656	0.9788
12 months	0.0353	0.0140	0.0290	0.0123	0.9340	0.9896
16 months	0.0403	0.0042	0.0353	0.0039	0.9506	0.9995
Overalldataset	0.0504	0.0133	0.0433	0.0114	0.9332	0.9953

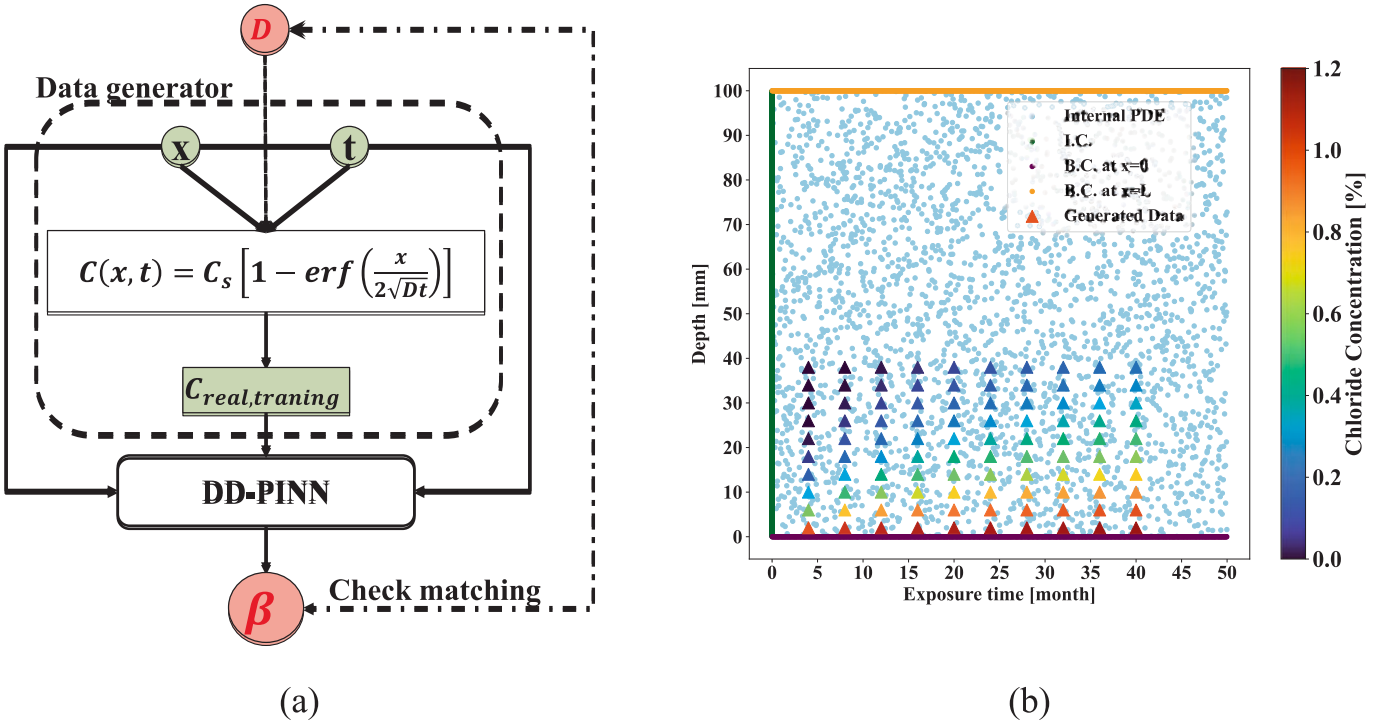

Fig. 11. (a) Data generator with constant D, and (b) generated 100 data points and sampling for PDE, I.C. and B.C.s in PINN.

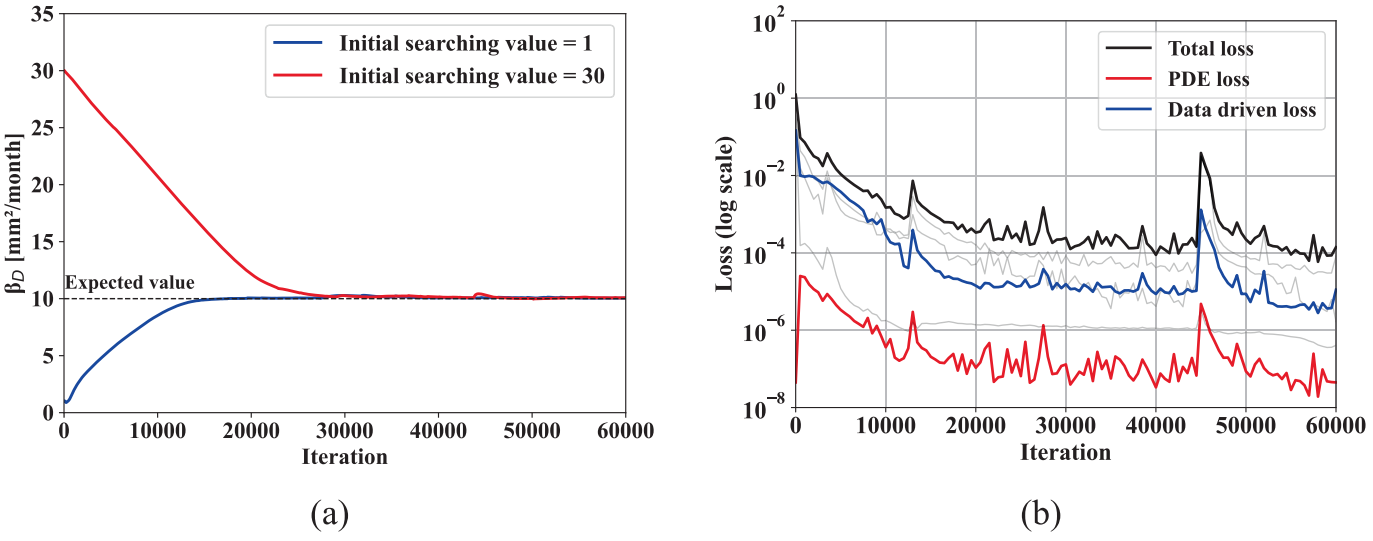

Fig. 12. (a) Coefficient estimated starting from different initial values, and (b) evaluation of training loss.

rapidly counter-perform the diffusion coefficient.

Estimating the diffusion coefficient by PINN requires an initial value for β. Fig. 12(a) shows that β starts searching from initial values of 1 and 30 mm^2/month respectively, and both eventually converge near the target value of $D = 10\,mm^2$/month, set for generating the data. This further demonstrates the accuracy of PINN for identifying the diffusion

coefficient. Searching from 1 is closer to the target value relative to searching from 30; thus, with the former initial value, the model calculations converge after less than 20,000 iterations. When inverting parameters via PINN, the network may yield multiple solutions resulting in an ill-posed estimation. The algorithmic code can restrict such ill-posed scenarios by incorporating a penalty term for loss through regularization strategies [46]. However, by setting the search range for diffusion coefficient estimation based on different concrete types (which can be regarded as an implicit regularization), this study avoids the occurrence of ill-posed estimation. For instance, the chloride diffusion coefficient for conventional Portland concrete is between 10^{-12} 10^{-10} m^2/s (equivalent to 2.6 260 mm^2/month) [47]. Therefore, it is significant to define a reasonable search scope; otherwise, the model's loss may converge, yet the prediction outcomes may deviate from reality. This is precisely why this framework necessitates the integration of engineering expertise. In addition, Fig. 12(b) shows the loss evolution over training iterations for this case, with the total loss approaching approximately 10^{-4}. A transient peak occurs near iteration 45000; the corresponding β exhibits only a small fluctuation at that point and is unlikely to materially affect the estimated value of β.

In practice, measured chloride concentration data in concrete are often affected by noise and uncertainty due to the inherent heterogeneity of the material and the complexity of the measuring environment. To address this issue, the robust noise immunity of the PINN model can be exploited. Specifically, during data generation, noise levels of 5%, 10%, 15%, and 20% were introduced into the generated data ($C_{noise,training}$) to simulate the fluctuations that may occur in actual measurements. The noise generation is using a multiplicative Gaussian noise model:

$$C_{noise,training}(x,t) = C_{real,training}(x,t)(1+\varepsilon), \varepsilon N(0,\tau^2) \tag{24}$$

where τ represents the relative noise level (coefficient of variation). The noise is independently sampled at each data point, and a fixed random seed is used to ensure reproducibility.

Subsequently, these datasets with varying noise levels were input into the PINN model to continuously estimate the chloride diffusion coefficient. Fig. 13(a) illustrates PINN identification of the diffusion parameter β under varying noise levels. On the noise-free dataset (0% Noise), the model converges precisely to the target value after approximately 15,000 iterations and maintains high stability around the expected value throughout subsequent training. This aligns with the loss evolution shown in Fig. 12(b): near the same position, both the PDE loss and data-driven loss have simultaneously decayed to extremely low levels. Thereafter, only minor oscillations characteristic of rapid convergence occurs, without adversely affecting the steady-state estimation of β. As noise increases, the β identified by PINN progressively deviates from the expected value and exhibits larger oscillations. This behavior is reflected in the loss curves shown in Fig. 14. For 5% noise (Fig. 14(a)), the total loss is dominated by the data-driven component and stabilizes near 10^{-3} As noise rises to 10%, 15% and 20% (Fi gs. 14 (b)–(d)), the data-driven loss establishes a lower bound that raises the total loss into the 10^{-2} range and increases fluctuations during parameter identification. It is important to emphasize that even under conditions of high noise, the PDE loss consistently remains at a low magnitude. This is because the PDE constraints are assigned higher weights, granting them greater dominance in the optimization process. This effectively suppresses the amplification effect of noise at the level of physical laws. This mechanism enhances the sensitivity of PINNs to the identification of diffusion parameters. Even when data quality deteriorates, the network can still maintain reasonable parameter estimates under the corrective influence of physical constraints. In other words, PDE constraints play a crucial stabilizing role in achieving steady-state parameter identification under noisy conditions.

To understand the potential errors arising from datasets with varying noise levels, each dataset underwent 10 repeated tests. The results are presented in Fig. 13(b). The experimental results show that when the data noise is low (in the range of 0% to 5%), the error of the model estimation results is less than 3%; even when the noise of the dataset reaches 15%, the estimation error can still be controlled within 10%. These quantitative findings demonstrate that the PINN model effectively mitigates the influence of noise on model outputs through its embedded physical constraint mechanism, thereby enhancing the stability and accuracy of the estimation results. This anti-noise capability provides a robust theoretical and experimental foundation for the practical application of PINN in complex engineering environments, ensuring high reliability even when data uncertainty is substantial.

Noise immunity was demonstrated using 100 data points generated by an error formula; however, obtaining this quantity of data in practical engineering tests entails significant time and cost. To assess the PINN model applicability with limited data, the sampling strategy used in actual chloride concentration studies was mimicked. Cuenca et al [48] investigated chloride diffusion in self-healing concrete, measuring concentrations at depths of 2.5 mm, 7.5 mm, 12.5 mm, and 17.5 mm after 1, 3, and 6 months of exposure, yielding 12 data points. These experimental data points were reproduced with 10% added noise; Fig. 15(a) presents the sampling and generated data points used in the PINN model. Across five consecutive training runs, convergence curves

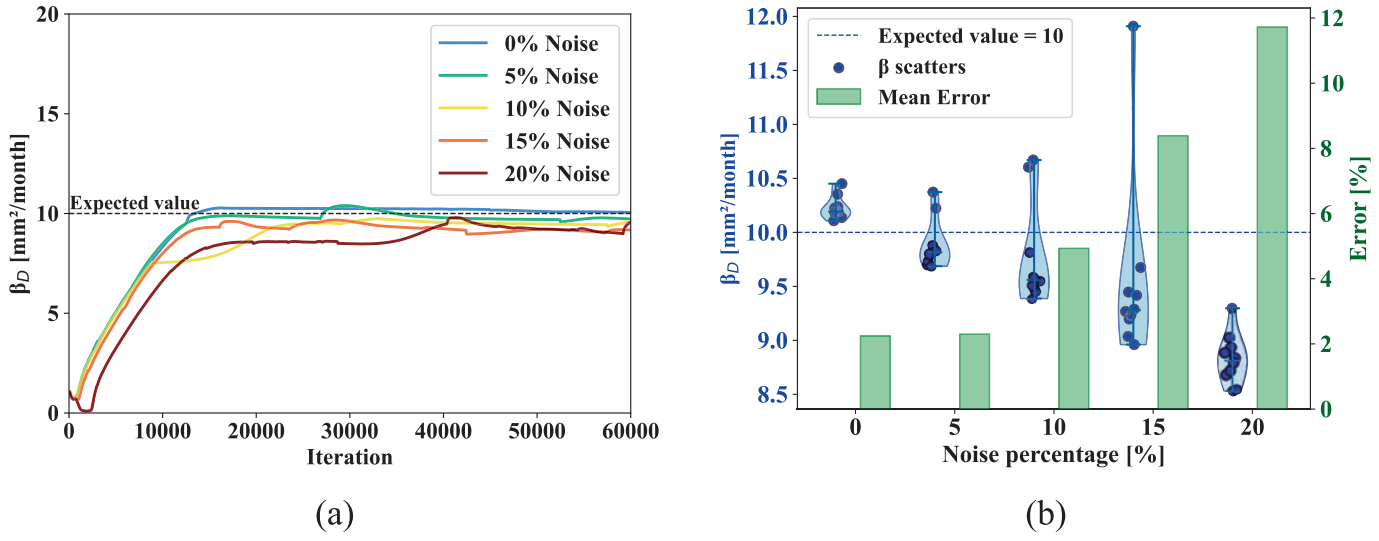

Fig. 13. (a) Estimating coefficient based on different noise level dataset; (b) 10 times repeated tests.

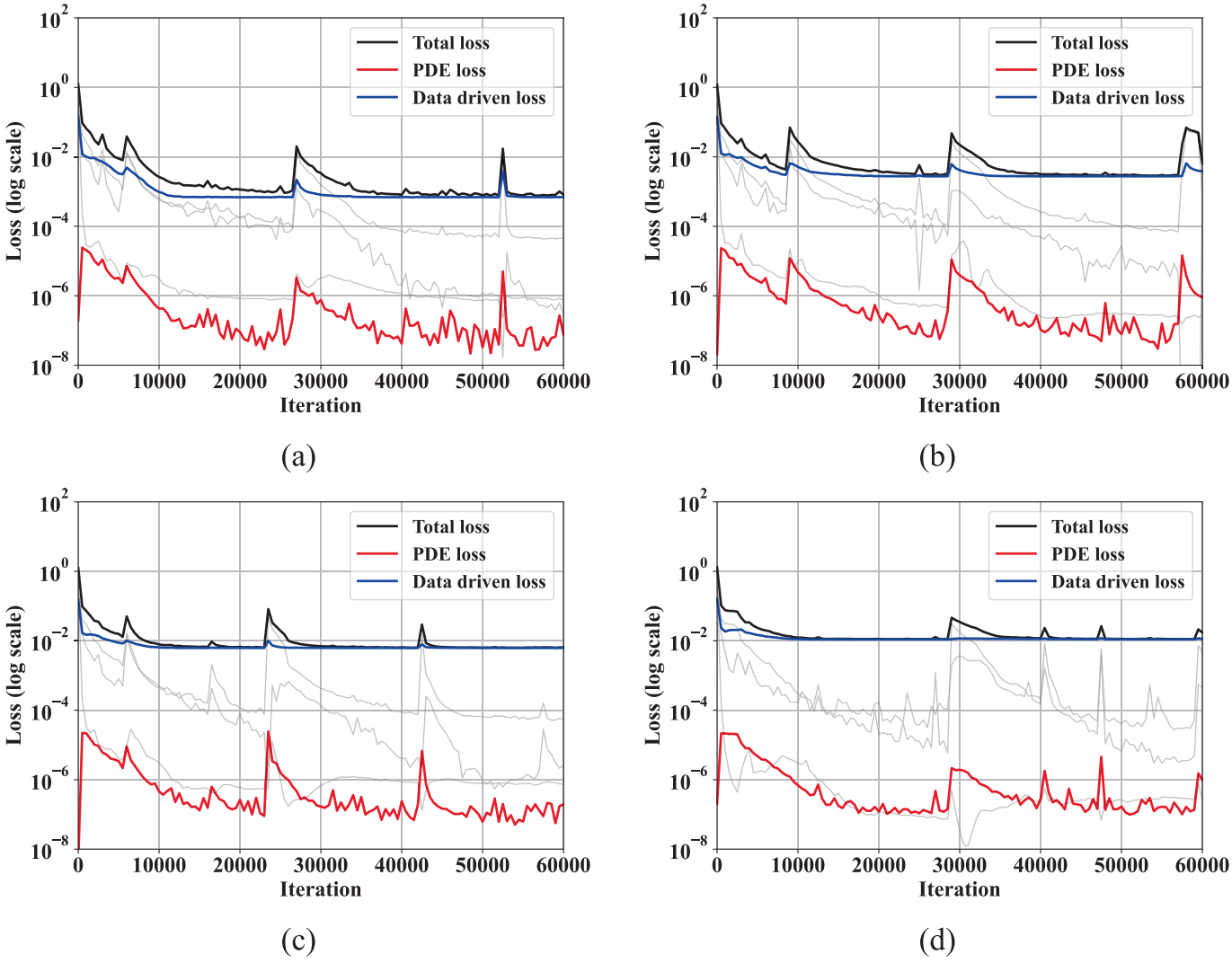

Fig. 14. Training loss of generated data at different noise levels: (a) 5%; (b) 10%; (c) 15%; (d) 20%.

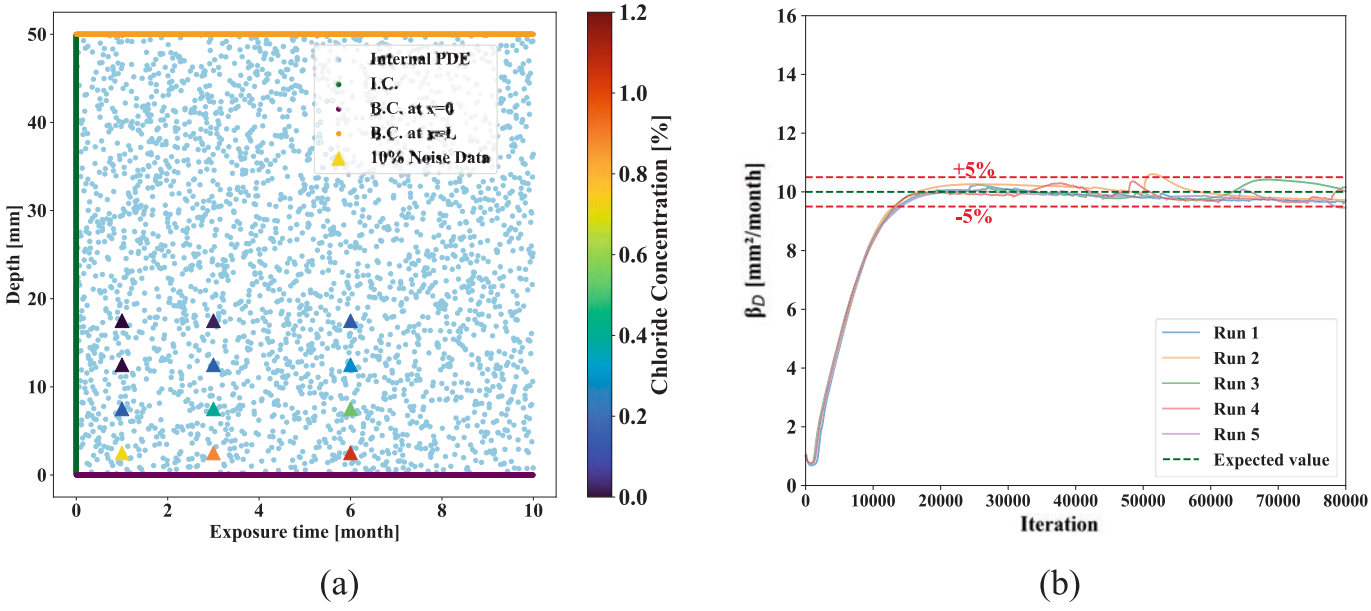

Fig. 15. Representation of the accurate behavior of the PINN in parameter estimation with low data availability.

stabilized within ± 5% of the expected values (see Fig. 15(b)), demonstrating that the PINN method maintains high inversion accuracy despite sparse and noisy data, and is suitable for studying natural chloride diffusion in concrete.

4.2.2. Estimating the dual parameter related diffusion

Considering that in a concrete matrix, the diffusion coefficient decreases with exposure time, Eq. (5) was used with two regression parameters, D_{ref} and n, which need to be obtained by fitting the chloride concentration dataset [35]. However, due to the complexity of the mathematical expressions in Eqs. (8) and (9), the fitting results are often unstable or yield multiple solutions. It is also worth noting that in many studies, the concentration–time relationship from Eq. (5) is directly substituted into Eq. (8) and then incorporated into Eq. (9), to account for the time-varying nature of the concrete diffusion coefficient. Although this approach simplifies the parameter fitting process, it may lead to inaccurate assessments of chloride diffusion behavior. Tang and Joost [37] identified challenges in various mathematical models of chloride diffusion and demonstrated that, under specific conditions, the apparent diffusion coefficients could be simplified to yield considerations analogous to those in Eq. (8). Boddy et al [38]. adopted an alternative simplification by setting the step size for calculating n to 0.1 in their diffusion model, to reduce computational complexity.

PINN has the potential to identify the dual-parameter problem described above, based on the dataset of chloride concentrations that has been collected. Its main advantage is the direct translation of the diffusion law into a loss term formed based on Eq. (1) without involving complex analytical formulas. In order to demonstrate the ability of PINN to recognize D_{ref} and n, Eq. (9) is first used to generate data in place of the experimental data collected in the actual tests (Fig. 16), and then the following assumptions were made: (a) $D_{ref} = 40mm^2/month$ when $t_{ref} = 28days \approx 1month$, (2) $n = 0.3$, (3) $C_s = 1.2\%$, and (4) the concrete exposure starts after its age of 28 days. Similar to previous procedures, diffusion depth, exposure time, and concentration values are integrated into the PINN model, and sequential parameter optimization is achieved through backpropagation. This approach captures subtle variations in the loss function while circumventing the resolution issues associated with an excessively large fixed step size of n.

Fig. 17 shows the convergence process of identifying the two parameters in Eq. (5) by DD-PINN. During the initial 10,000 iterations, the model undergoes a trial phase, gradually converging toward the target values. The final estimated or identified parameter values are very close to those set in the data generator. This demonstrates the feasibility and accuracy of the PINN model in addressing this type of problem. To prevent multiple solutions, it is essential to define an appropriate search range. Literature indicates that the parameter n primarily depends on the mixture design: for ordinary Portland cement, n typically falls within the low range (< 0.3), whereas values in the high range (0.5–0.7) are associated with the normal replacement levels of fly ash and slag [38,49,50].

The approach used by Thomas and Bamforth [49] was to select the values of D_{ref} and n as input variables to the model, with n calculated in steps of 0.1, in order to best fit the experimental curves for each sampled

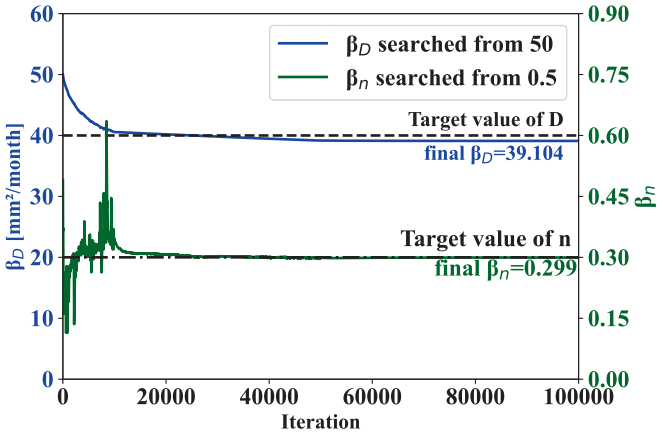

Fig. 17. Identification of the dual parameters based on data generator.

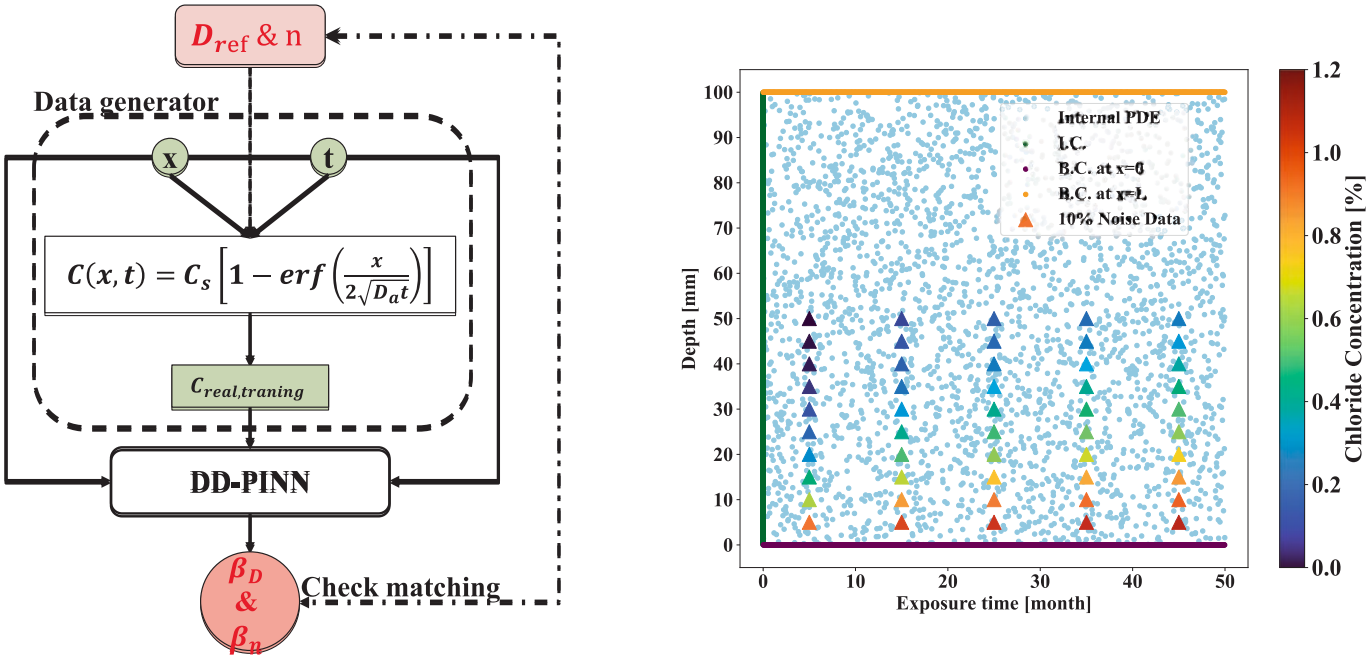

Fig. 16. (a) Data generator with $D(t)$, and (b) generated 50 data points and sampling for PDE, I.C. and B.C.s in PINN.

age. The best fit criterion defined by them was the sum of the squared errors between the model predictions and the experimental data at all the exposure times. Fig. 18 shows the values of the parameters calculated through the PINN model for conventional concrete and fly ash concrete, respectively. The advantage through this method is that it avoids the use of complex analytical solutions based on Fick 2nd law (Eqs. (8) and (9) for fitting. In particular, there is no need to carry out a discussion on the influence of the $\frac{f(t_{ex})}{1-n}$ term on the results. Many studies have ignored this term and used oversimplified mathematical models for the study [37]. Unlike the oversimplified models, the PINN model is built to strictly conform to the physical laws of diffusion, and the final predictions generated are also in agreement with the actual measurements, see Fig. 19.

4.3. 2D problem: Applications to cracked concrete

In this section, the proposed PINN framework is applied to concrete systems containing cracks. Section 4.3.1 employs cracked concrete as a benchmark case for diffusion simulation, providing an approach to solving a two-dimensional forward problem. Section 4.3.2 extends this methodology to self-healing concrete to evaluate its capability in estimating key healing parameter.

Consideration of chloride diffusion in cracked concrete requires the extension of the diffusion behavior to a two-dimensional model of the concrete multiphase. In general, in many simulation experiments, the crack is assumed to be straight [7,8]. In a two-dimensional time-varying model, the limitation of the high computational cost of PINN is magnified as the number of sampling points increases, and the performance of the model is extremely dependent on a large number of operations to achieve convergence [30]. Therefore, it is necessary to make a simplified treatment of the diffusion of chloride in cracked concrete, through the following steps: (1) simplifying the diffusion phases of chloride in concrete; (2) simplified analysis by shape symmetry; (3) applying a dual-domain PINN.

This paper only investigates chloride diffusion in the concrete phase and in the crack phase. Assumptions regarding the crack location and path are made as represented in Fig. 20. It can be noted that the cracks are always in the middle of the concrete matrix (like in a splitting test in Fig. 2) and only propagate in one direction akin to a penetrating effect without any bending. In addition, the experimental data are taken into consideration to be also incorporated into the model for the study of inverse problems related to estimating the diffusion coefficients, and the conditions of the concrete specimens treated in the tests (in Section 2.2) are strictly followed to construct the boundary conditions and the initial conditions of the chloride diffusion in the cracked concrete:

$$\begin{cases} u(x,y,t=0)=0 \\ u(x=0,y,t)=C_s(t) \\ \left.\dfrac{\partial u}{\partial x}\right|_{x=L}=0 \\ \left.\dfrac{\partial u}{\partial y}\right|_{y=0}=\left.\dfrac{\partial u}{\partial y}\right|_{y=L}=0 \end{cases} \tag{25}$$

Fig. 20 presents a schematic diagram of the crack and concrete. The unidirectional diffusion and inherent symmetry of the specimen enable a reduction in the computational domain of the PINN model by analyzing the half zone. Moreover, to capture the contribution of concrete's self-healing function to resisting chloride diffusion, the crack width is constrained within a healing range ($\leq$ 0.3 mm) [51,52]. Since the width of the cracks is much smaller than the dimensions of the concrete, the diffusion coefficient also varies considerably. In this study, an independent PINN of subdomain is established for the concrete and cracked phases to form a dual-domain PINN model (also known as an extended PINN (xPINN) model [30,31]), including concrete-PINN (Con-PINN) and crack-PINN (Cr-PINN), which is used to cope with the challenge of different diffusion characteristics and size effects in the concrete and cracked phases. In order to create a communication between each other, the interfacial boundary conditions between the two subdomains should satisfy the basic physical principles of diffusion: (1) concentration consistency and (2) flux consistency. The expression for this physical relationship is given below:

$$\begin{cases} u_{Con-PINN}(x,y_{inter},t)=u_{Cr-PINN}(x,y_{inter},t) \\ D_{con}\bullet\left.\dfrac{\partial u_{Con-PINN}}{\partial y}\right|_{y_{inter}}=D_{cr}\bullet\left.\dfrac{\partial u_{Cr-PINN}}{\partial y}\right|_{y_{inter}} \end{cases} \tag{26}$$

where $u_{Con-PINN}$ and $u_{Cr-PINN}$ represent the predicted value by Con-PINN and Cr-PINN, respectively, and y_{inter} indicates the interfacial line between the crack phase and concrete matrix.

Furthermore, as the total loss of xPINN comprises multiple components (subdomain PDE residuals, boundary/initial conditions, and interface matching terms), these terms may differ by several orders of magnitude. This disparity hinders optimizers from simultaneously minimizing all components, resulting in suboptimal fitting of concentration fields near the interface [30,53]. In this study, the loss curves and prediction results for the xPINN not incorporating data generated by the FEM can be found in Appendix B. It is evident that although the loss

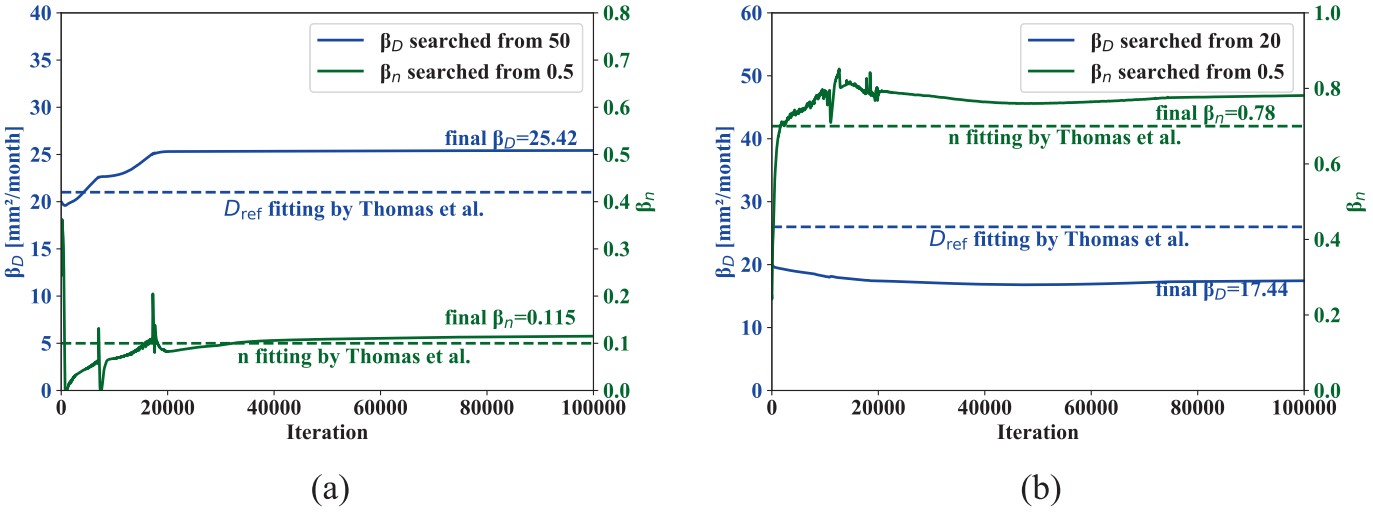

Fig. 18. PINN Identification of the dual parameters, compared with fitting methods: (a)OPC, (b)FA.

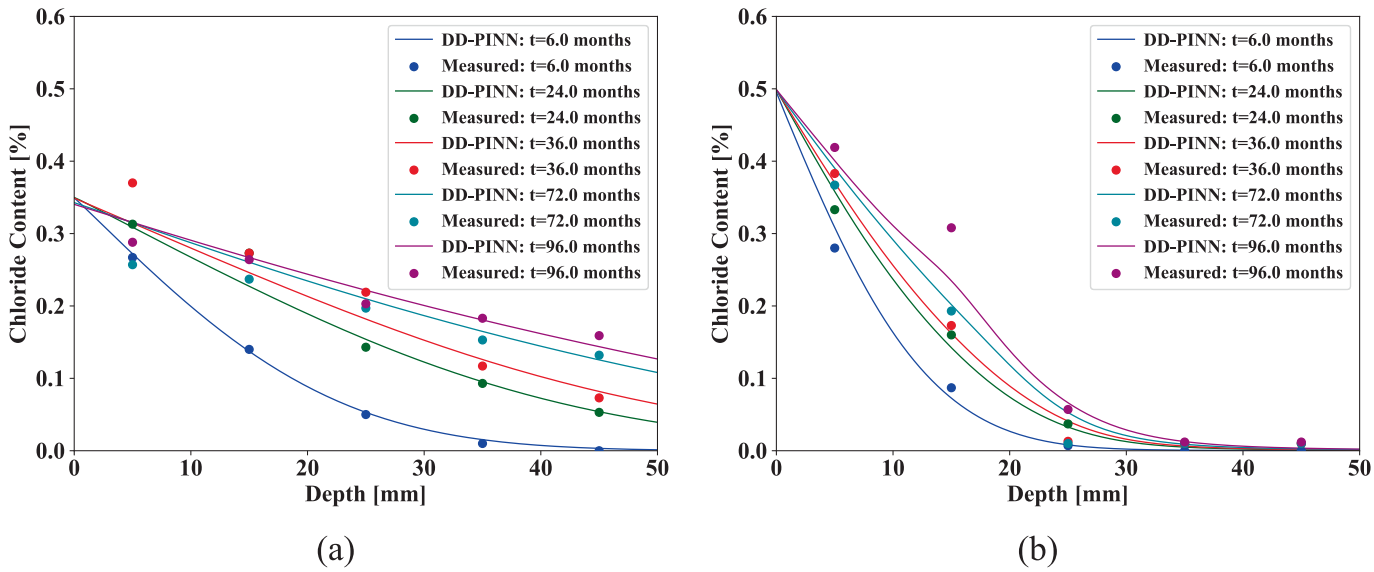

Fig. 19. Comparison between DD-PINN and measured data by Thomas and Bamforth [49]: (a)OPC, (b)FA.

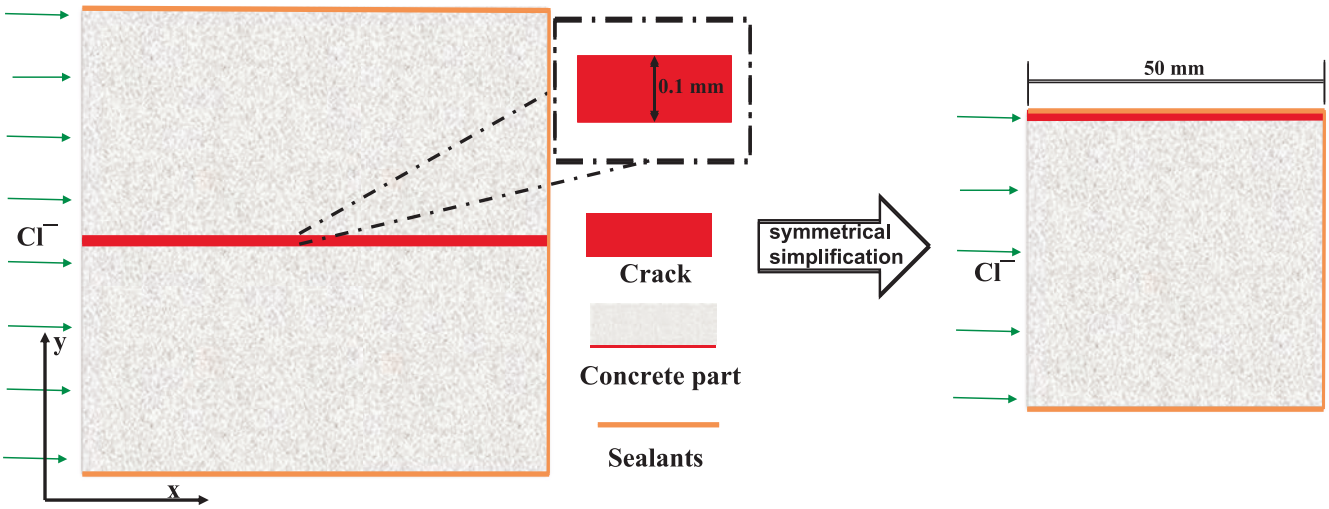

Fig. 20. Schematics of chloride transport in cracked concrete and simplified considerations in modelling.

curve eventually flattens (Fig. 32), the prediction quality (Fig. 33) falls significantly short of the supervised xPINN results (Fig. 25). To address this issue, high-fidelity finite element data or experimental data at the interface are introduced as a supervision term, thereby transforming the pure xPINN into a weakly supervised xPINN [54]. This approach has been demonstrated to improve the loss scale and enhance the convergence of the interface solution.

The final loss convergence process for the PINN model in each subdomain includes the loss values corresponding to each term in Eq. (20), along with the interface loss composed of concentration consistency and flux consistency as defined in Eq. (26). Finally, an indicator function is introduced to balance the concentration solutions at the boundary of the two subdomains interface, while stitching together the global solution [30]. This function is defined as:

$$\mathbb{I}_{\Omega(x,y)} = \begin{cases} 0, if(x,y) \notin \Omega_{sd} \\ 1, if(x,y) \in \Omega_{sd} \backslash commoninterfacein\Omega_{sd} \\ \frac{1}{N_{sd}}, iff(x,y) \in commoninterfacein\Omega_{sd} \end{cases} \tag{27}$$

in which N_{sd} is number of subdomains (in this case, $N_{sd} = 2$) and Ω_{sd} is the zone of one subdomain. Note that, in order to reduce the consumption of computational resources, individual models need to converge before the merged model is built.

4.3.1. *Predicting diffusion in cracked concrete*

When chloride diffuses in ordinary cracked concrete, it is straightforward to classify this diffusion behavior as being in the cracked phase and the concrete phase. In order to predict the diffusion behavior of chloride using a dual-domain PINN, reference is made to the experimental results of Djerbi et al [55]. The diffusion coefficient of the concrete phase is 4.7mm^2/month, and the diffusion coefficient of the cracked phase is related to the width of the cracks as follows:

$$D_{cr}(w) = \begin{cases} 52 \bullet w - 1036 mm^2/month, 30 \le w \le 80 \mu m \\ 3628 mm^2/month, w \ge 80 \mu m \end{cases} \tag{28}$$

The simulation procedure of the two domain PINN is illustrated by introducing a crack of width 0.10 mm (0.05 mm after exploitation of symmetry) and imposing the surface concentration of Eq. (23). This is

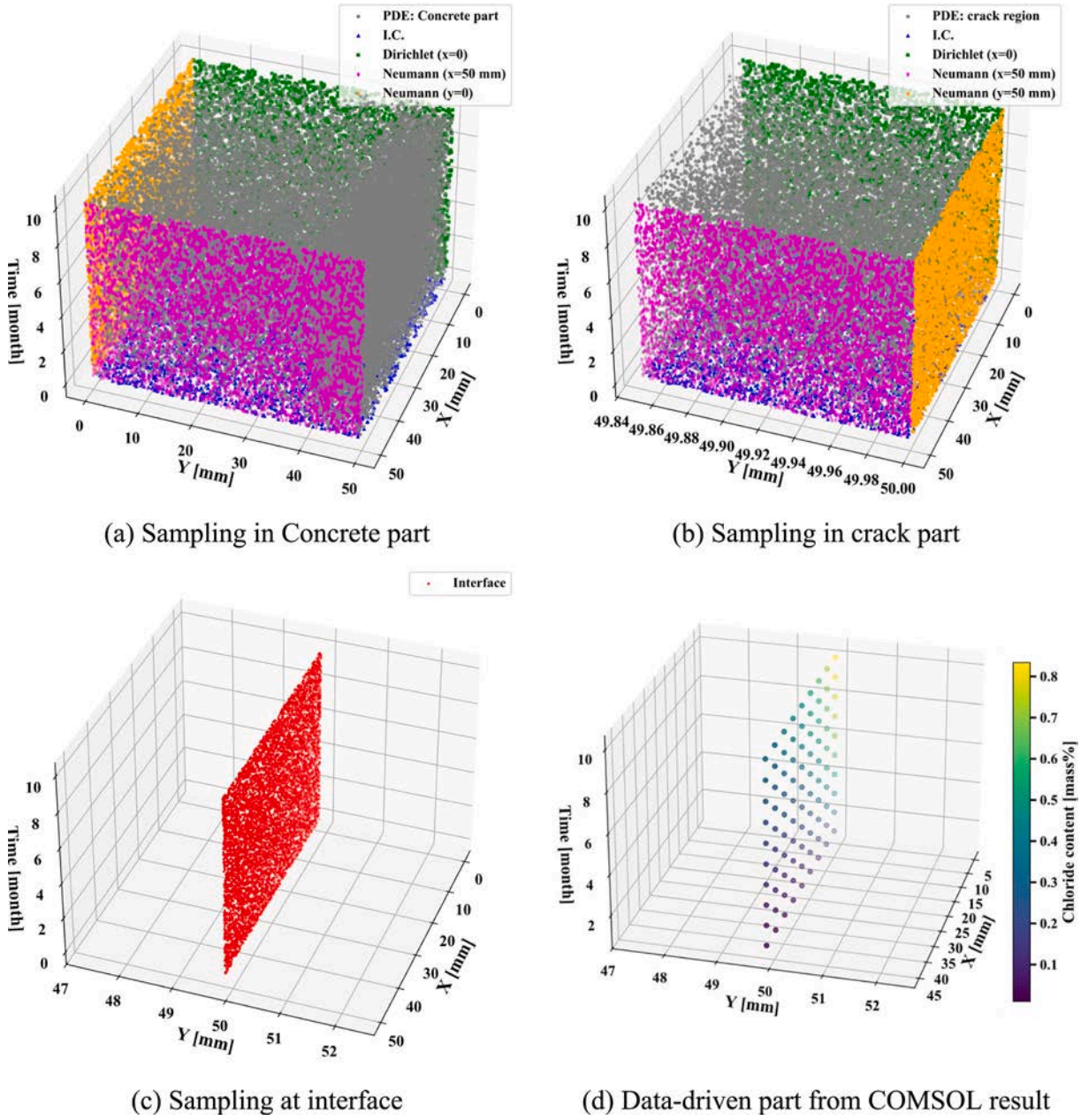

Fig. 21. Sampling in PINN includes (a), (b), (c), and COMSOL output data (d).

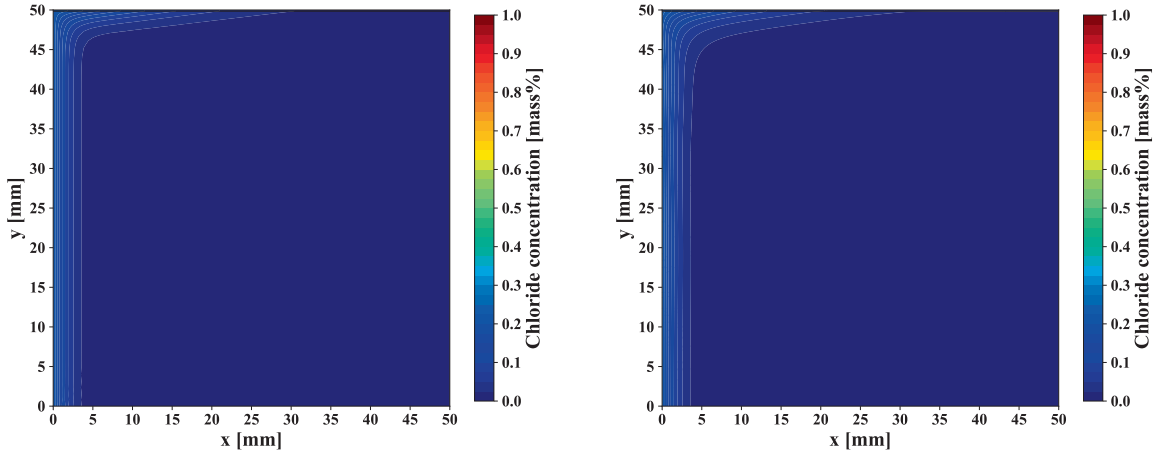

(a) 1-month exposure, COMSOL result (b) 1-month exposure, xPINN model result

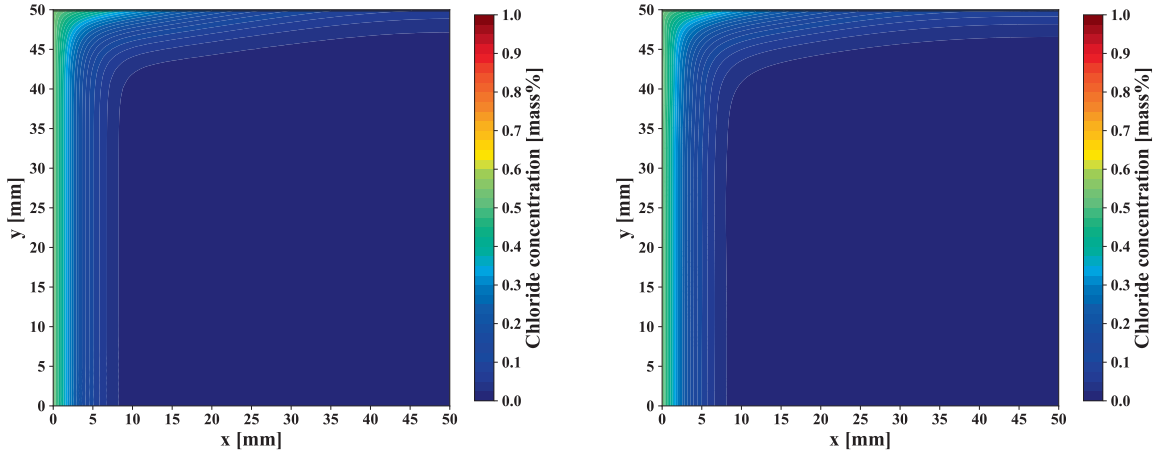

(c) 3-month exposure, COMSOL result (d) 3-month exposure, xPINN model result

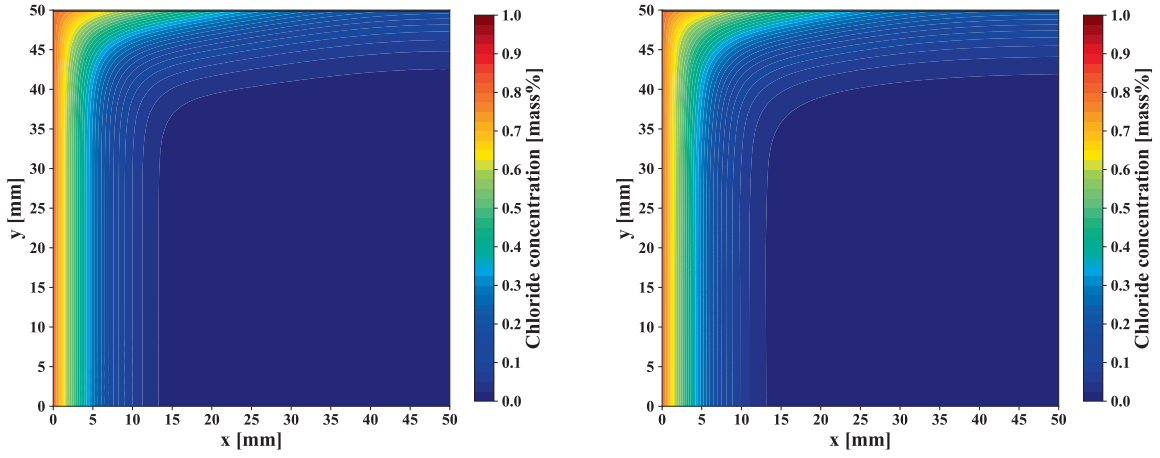

(e) 6-month exposure, COMSOL result (f) 6-month exposure, xPINN model result

Fig. 22. Chloride concentration contour in concrete with straight crack, as obtained with the xPINN model and COMSOL.

done to ensure an appropriate healing performance within the cracked concrete specimens. This smaller crack-width is also advantageous in avoiding higher diffusion induced by the surrounding water pressure within the crack-zone. To strengthen the coupling at the subdomain interface, the following strategies were implemented:

17 **Refined collocation near the crack**. In the concrete domain, division along the y-axis enables dense sampling: 16,000 collocation points over 0–39.88 mm and 16,000 over 39.88–49.85 mm (Fig. 21a). Further 4000 points enforce the governing PDE at the domain boundaries and at initial time

18 **Enhanced interface sampling**. 8000 collocation points were placed directly at the interface to improve information exchange between subdomains (Fig. 21c). The sampling strategy here has the same objective as the local refinement of the meshing around the cracks in the finite element method to achieve more accurate predictions

19 Data-driven enrichment. The construction of COMSOL model is choose the transport of dilute Species as a study Physics, and conditions follow the Eq. (25). COMSOL-generated concentration data (as high fidelity data [56,57]) were incorporated as supervised training points in the model data-driven branch (Fig. 21d)

20 **Staged training.** The Con-PINN and Cr-PINN parts are trained independently, and then the loss terms in Eq. (26) are added to train the two networks jointly. Note that the interface loss is a separate component and is only incorporated into the total loss during joint training. The relevant algorithm could be found at Appendix A

Fig. 22 presents the modelling results for both simulation methods at 1-, 3-, and 6-month time periods. The predictions of both methods closely coincide, with only minor discrepancies at localized regions near the interface arising from interactions between Con-PINN and Cr-PINN physical constraints. Consequently, precise coordination between the two networks is essential for accurate and reliable predictions when applying the xPINN method to cracked concrete. Incorporating fidelity data at the interface can enhance the model's expressive capability. In regions distant from the crack, both methods yield nearly identical results, as these areas remain largely unaffected by the intensified diffusion within the crack domain.

In addition, the PINN solution exhibits smoothly stratified concentrations, whereas the FEM solution may display angular discontinuities or stepwise gradient jumps at element interfaces, giving it a rougher appearance depending upon the refinedness of the meshing. This contrast stems from their fundamental methodologies: PINN employs a global neural network approximator (see Eq.10) that inherently enforces smooth transitions via successive activations functions, even across concentration mutations. In contrast, FEM partitions the domain into finite elements and represents the solution within each cell using polynomial basis functions (e.g., linear or quadratic). Although the solution values remain continuous at cell boundaries, their derivatives frequently become discontinuous.

Fig. 23(a) shows a sampling line established along the crack opening, extending downward and diagonally into the concrete interior to capture chloride diffusion from the crack into the substrate. This line provides a continuous depth profile spanning the crack–concrete interface and the concrete interior, simultaneously capturing elevated chloride concentrations within the crack and their inward diffusion based on predictions from the two subdomain models. To further validate model accuracy, approximately 200 data points along this diagonal profile were extracted from both the xPINN and COMSOL simulations (Fig. 23 (b)). The xPINN predictions closely match the COMSOL outputs at each sampling location ($R^2 = 0.99$), with both MAE and RMSE remaining very low. These results demonstrate that the model effectively simulates chloride transport from the crack opening into the concrete interior.

In practice, cracks often exhibit curvature, and the dual-domain xPINN approach presented here likewise holds significant potential for analyzing such geometries. To simplify the procedure, assuming an idealized curved crack as shown in Fig. 24, sampled analogously to the straight-crack case in Fig. 21. It should be further emphasized that, as the concentration gradient along the central axis of the curved crack is not symmetrical on both sides, practical considerations necessitate more rigorous and complex treatment of boundary conditions at the symmetrical central axis when applying symmetrical simplifications. The objective of this study is to enhance the information and computational coupling between the curved crack domain and the rectangular concrete domain. Therefore, the zero-flux boundary condition is maintained at the symmetrical central axis.

Fig. 25 presents the chloride concentration distribution after 2, 4, and 8 months of exposure. The xPINN model's predictions closely match those of the FEM, demonstrating xPINN strong potential for modelling chloride diffusion in cracked concrete. It can also be noted that the xPINN model has a higher accuracy in prediction the chloride diffusion in case of cracks with higher tortuosity. The future application of this

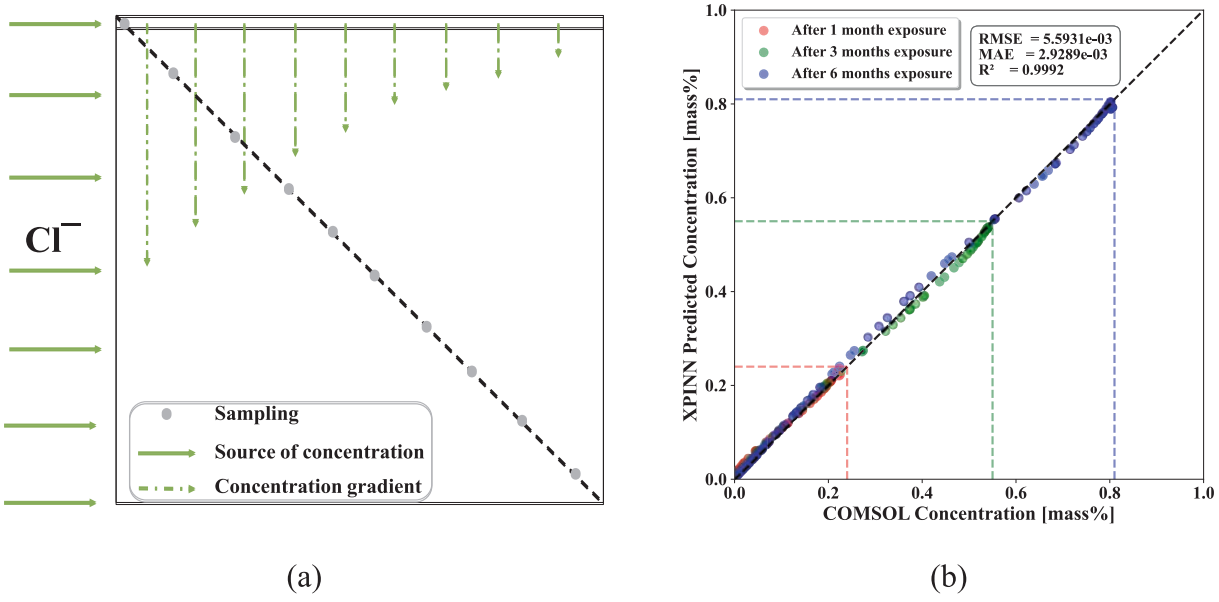

Fig. 23. (a) Sampling at the diagonal line for validating the accuracy of xPINN, and (b) parity plot to compare along the diagonal line the xPINN and COMSOL solutions.

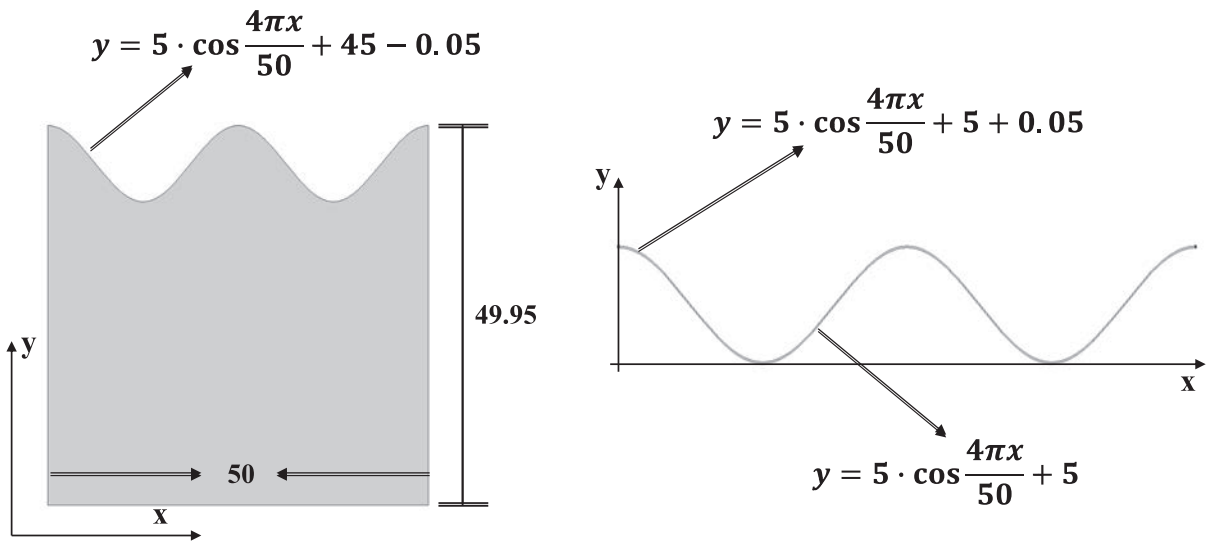

Fig. 24. Designing an ideal tortuous crack with width of 0.05 mm after symmetrical processing.

work can be extended to concrete systems with higher crack tortuosity such as fiber-reinforced concrete and 3D printed concrete with complex geometries.

4.3.2. Research framework for the analysis of self-healing concrete

Considering concrete's self-healing functionality, the diffusion coefficient within cracks evolves with healing time, complicating the modelling of chloride diffusion in self-healing concrete. In this study, an expression (see Appendix C) was derived to characterize the variation of the diffusion coefficient inside the crack during healing. Leveraging two-domain PINN inversion, the primary objective was to estimate the fully healed crack diffusion coefficient D_{CA}. To complement this approach, chloride concentration results from Cuenca et al [48], see Fig. 26, were incorporated in the study, to inform the local PINN reconstruction and enhance data interaction at the interface; the complete experimental dataset is provided in Appendix D.

Fig. 27 illustrates the study framework for the diffusion problem of self-healing concrete. Chloride data from the experimental results in Fig. 26 were divided into two groups (A and B) located away from the cracks; these groups were largely unaffected by crack-induced concentration gradients. Consequently, these data points were used to estimate the diffusion coefficient of the undamaged concrete following the PINN-based inverse approach described in Section 4.2.1. Additionally, modelling chloride diffusion required determining the surface chloride concentration, which was fitted using the exponential formula in Table 2 (details in Section 2.2), with results presented in Fig. 28(a). The diffusion coefficient for this concrete phase, determined upon convergence of the DD-PINN model, is shown in Fig. 28(b) as 2mm^2/month for the concrete matrix.

Group C serves as interfacial concentration data for the data-driven component of the model, facilitating faster convergence at critical locations and compensating for the limited constraints imposed by purely physical residuals on the interface region compared to the fidelity data exported from COMSOL in Section 4.3.1. However, these data points are subject to noise from the experimental measurements. Moreover, in Cuenca et al.'s chloride test [48], Group C was positioned slightly farther from the crack than depicted in Fig. 26, so it does not accurately represent the actual interfacial concentration. Consequently, a data-driven error arises in estimating the fully healed crack's internal diffusion coefficient D_{CA} relative to its true value. More precise diffusion coefficient estimations depend on improved laboratory methodologies and higher-quality test data i.e., samples taken closer to the crack-concrete interface. This study's primary objective is to demonstrate the feasibility of the multi-domain PINN approach for modeling chloride diffusion in self-healing concrete. Therefore, based on this approach, by substituting laboratory data for high-fidelity data, the model can fulfil its role in guiding and designing laboratory work. Through the requirements for data points within the xPINN, the test locations for chloride diffusion experiments can be correspondingly adjusted.

After determining the concrete diffusion coefficient, the FEM guides the PINN model by defining the search range for diffusion coefficients. The fully healed crack diffusion coefficient was estimated via FEM to be approximately 10–100 times larger than that of the uncracked concrete (Fig. 29(a)). This pre-calculated range is used to constrain the network search and thus significantly reduce the xPINN model's computational cost. Furthermore, the FEM-based inversion process involves iterative forward simulations followed by manual or external parameter adjustments based on the error between simulation and measurement, repeated until convergence. This provides a systematic solution to the parameter-identification problem in this study. Within the proposed framework, FEM therefore acts as a high-fidelity forward solver that both supplies reliable prior information for constraining the PINN inversion and serves as a reference for validating the learned diffusion parameters.

Fig. 29(b) shows the results of the search starting from different starting values (50mm^2/month and 100mm^2/month), and both the final results converge to 74mm^2/month. This demonstrates that for inversion problems of this nature, within the framework presented in Fig. 27 and under conditions where a reasonable search parameter range is specified, the weak constraints provided by experimental data assist the network in resolving the inversion problem without encountering significant instability. This value was then entered into COMSOL, and Fig. 30 presents concentration contour plots from the COMSOL simulations alongside xPINN predictions at 1, 3, and 6 months. The two sets of predictions closely agree. As exposure time increases, self-healing reduces the chloride transport across cracks; the chloride flux from the crack domain into the concrete domain diminishes along with the concentration gradient, and both models effectively capture this healing effect.

Fig. 31 presents the concentration at the interface versus time for

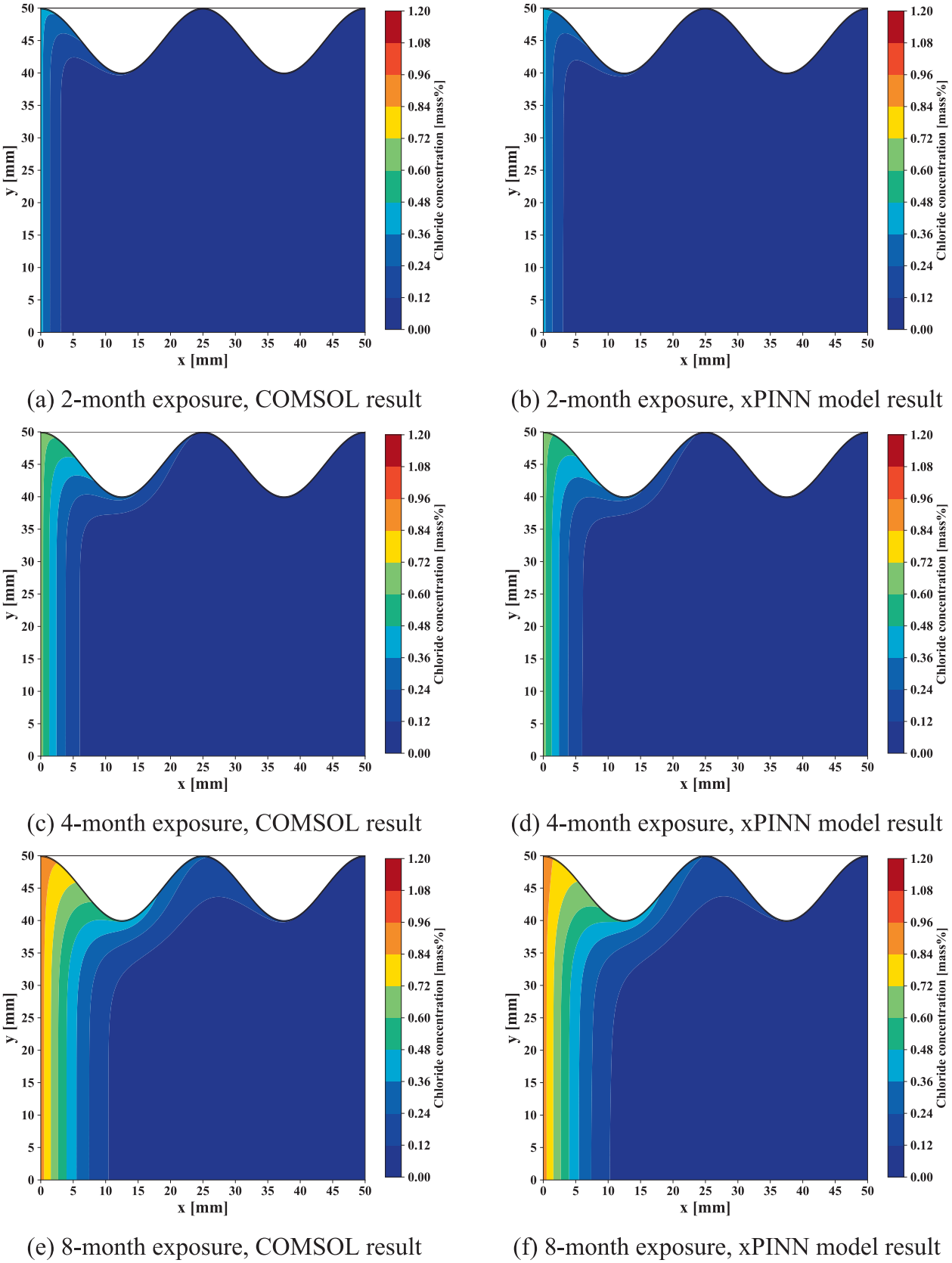

Fig. 25. Chloride concentration contour in concrete with ideal curved crack, as obtained with the xPINN model and COMSOL.

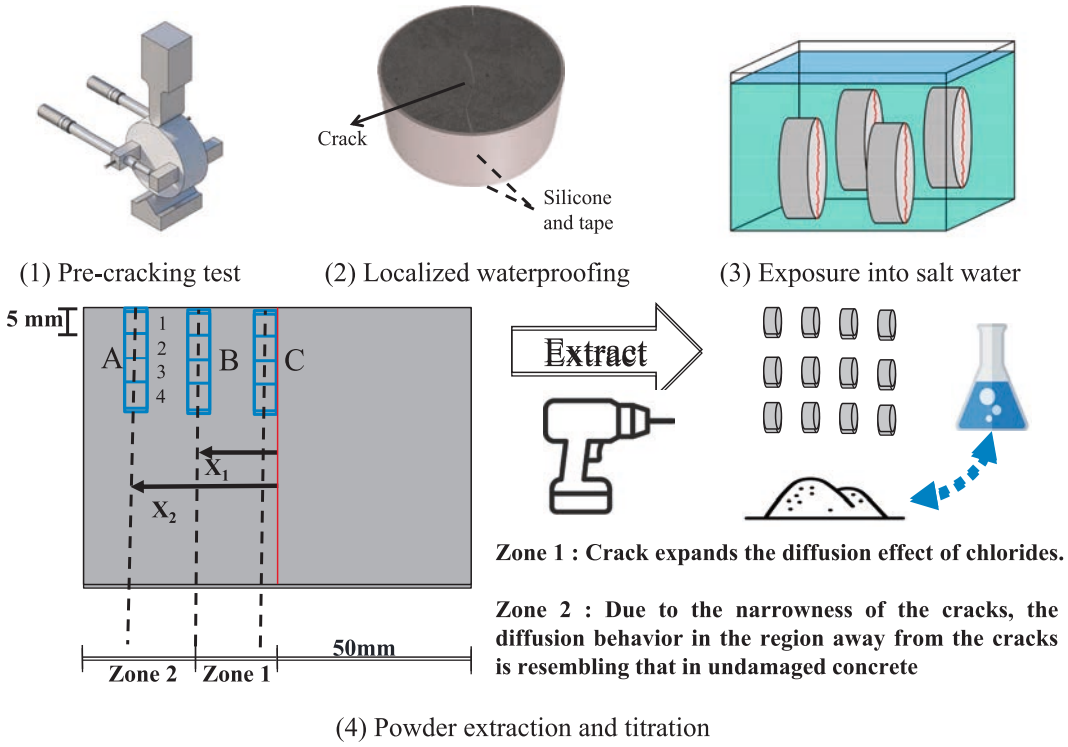

Fig. 26. Experiments work for providing the chloride data of self-healing concrete.

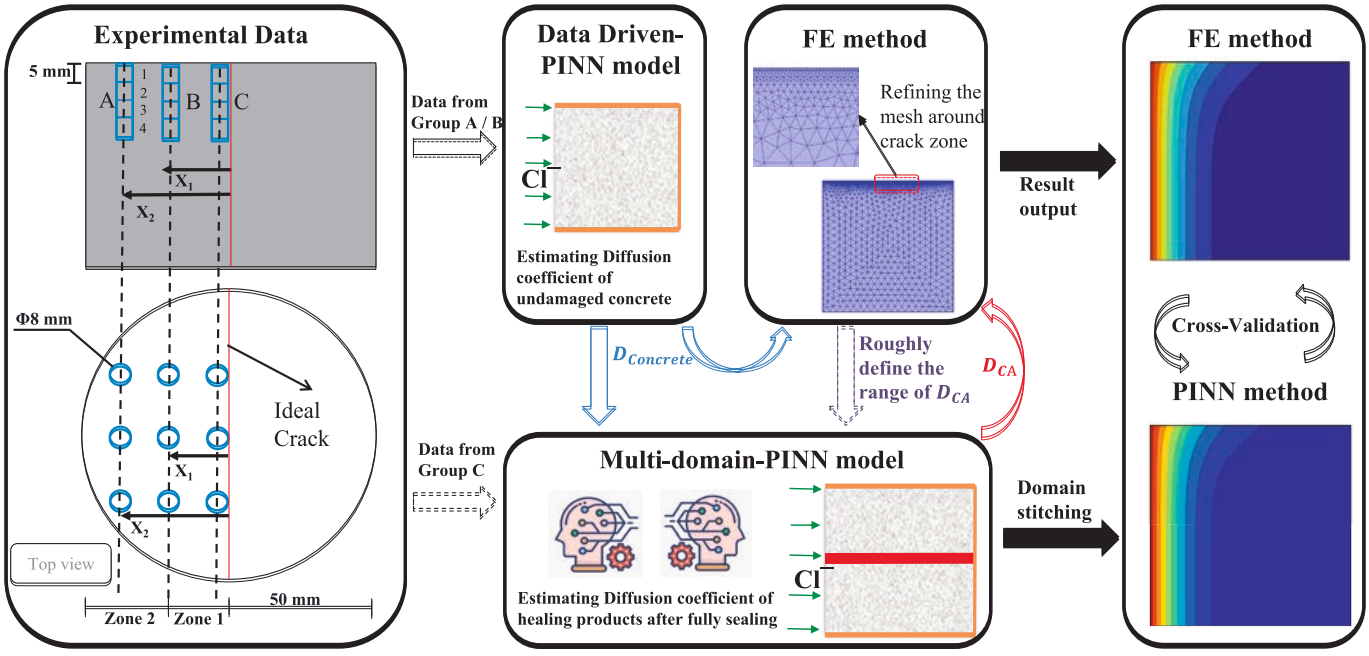

Fig. 27. Research framework for chloride diffusion in self-healing concrete.

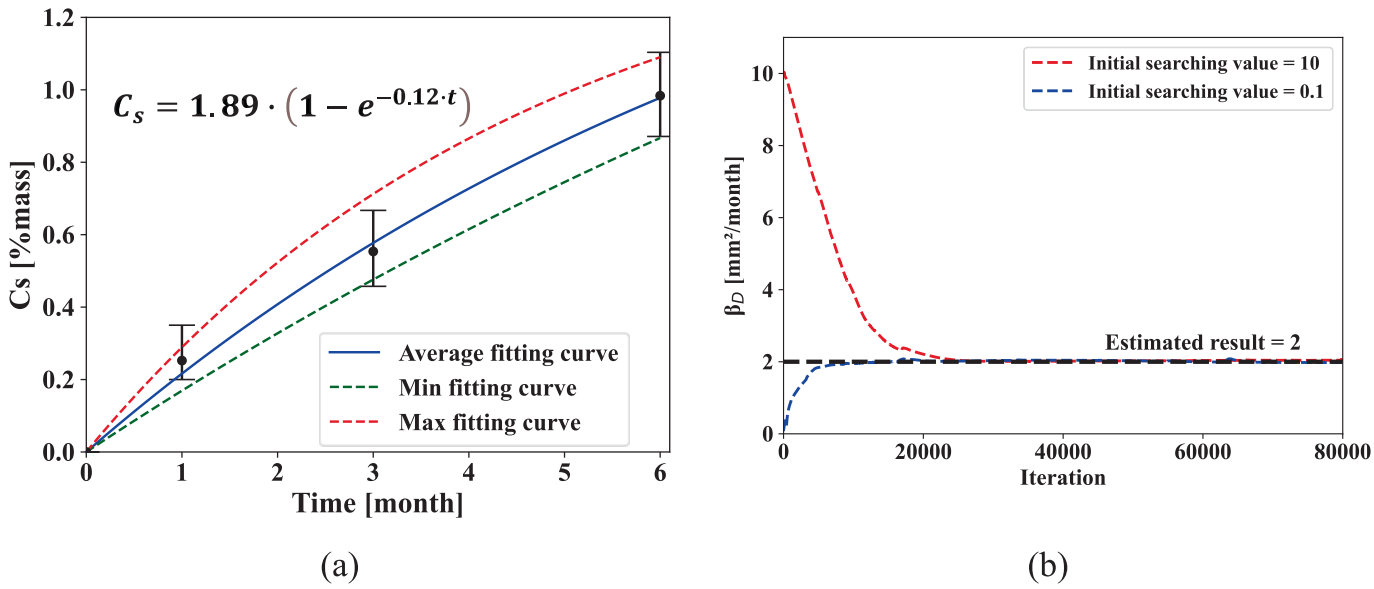

Fig. 28. (a) Fitting the surface concentration by publication of Cuenca et al, and (b) diffusion coefficient of concrete undamaged part estimated moving from different initial values.

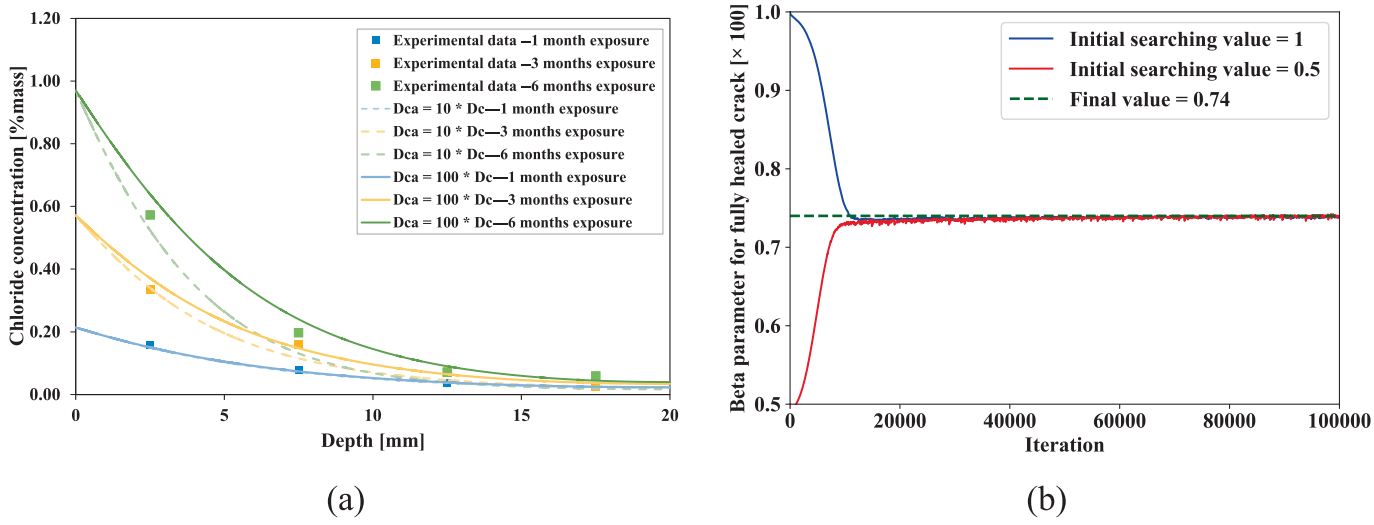

Fig. 29. (a) Rough estimation of diffusion coefficients of fully healed crack D_{CA} by manual attempts of COMSOL, and (b) fine estimation of the convergence process of D_{CA} using the multi-domain PINN model.

both models. Overall, xPINN provides a closer fit to the experimental data than COMSOL, particularly at shallow depths (x < 10 mm) where the concentration gradient is steepest, after 3 and 6 months of exposure. xPINN more accurately reproduces the decay rate, whereas COMSOL systematically overestimates it.

This discrepancy likely arises because xPINN incorporates experimental boundary conditions and physical constraints during training, allowing it to tune diffusion coefficients and reaction rates directly, while COMSOL relies on preset physical parameters and numerical discretization, which accumulate error in regions of moderate to high concentration gradients. In addition, RMSE, MAE and R^2 were used to assess the error metrics of COMSOL and xPINN with respect to the experimental data (see Table 5). After one month of exposure, COMSOL excels at capturing rapid variations in shallow compartments due to its fine grid and calibrated physical parameters. By three months, xPINN matches COMSOL within learned constraints. At six months, xPINN outperforms COMSOL on all metrics, demonstrating that its data-driven, physics-informed framework continuously refines parameters and surpasses traditional FEMs in predicting long-term diffusion behavior which is important for sustainable design considerations.

5. Conclusion and future work

This paper has systematically evaluated the performance and application potential of a PINN based on Fick 2nd law for modelling chloride diffusion in concrete through numerical simulations and experimental validation. The main contributions and conclusions are summarized as follows:

(1) **PINN model fusion with experimental data:** in one-dimensional diffusion simulations, the physically driven P-PINN

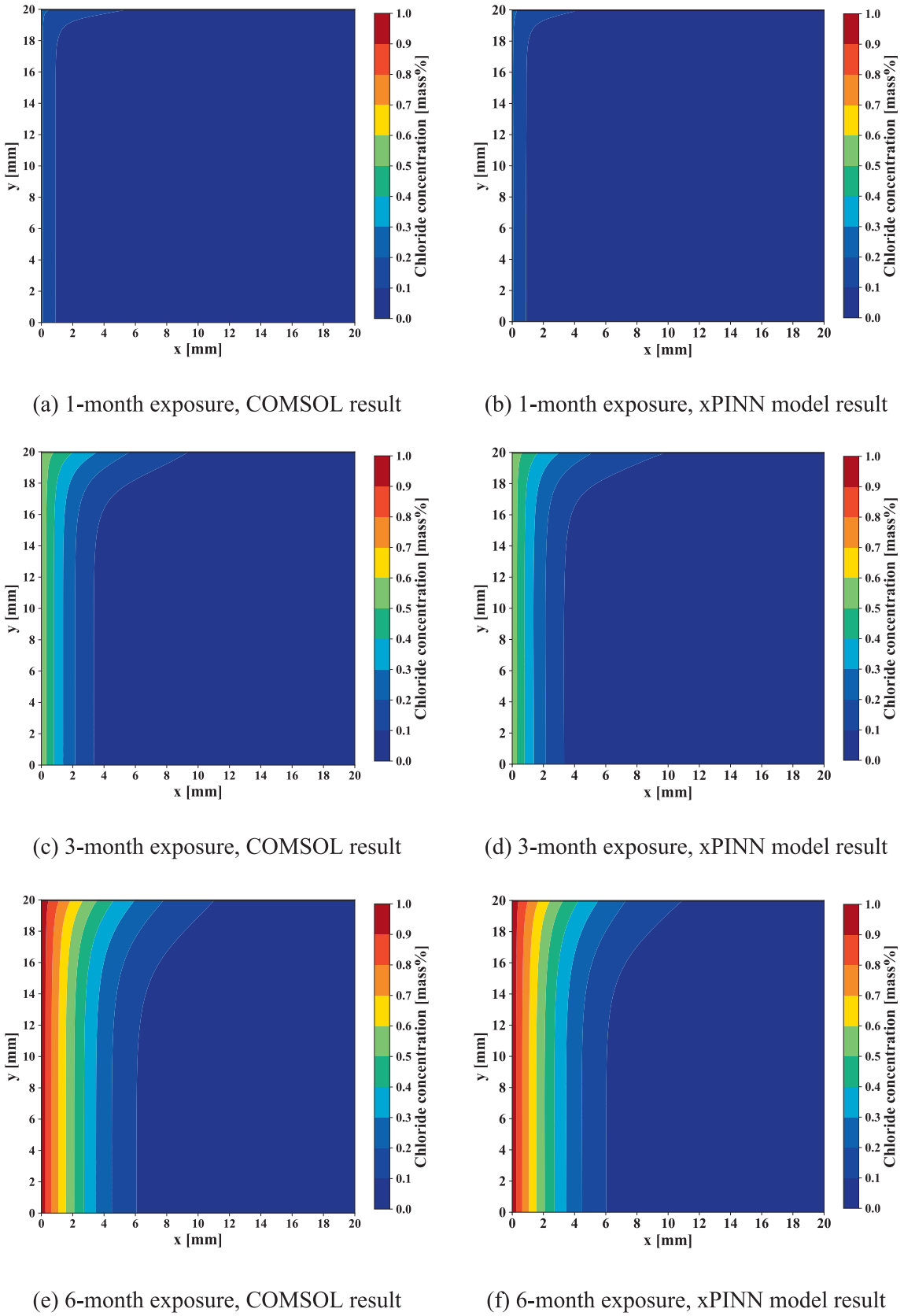

Fig. 30. Chloride contour in self-healing concrete, as obtained with the xPINN model and COMSOL.

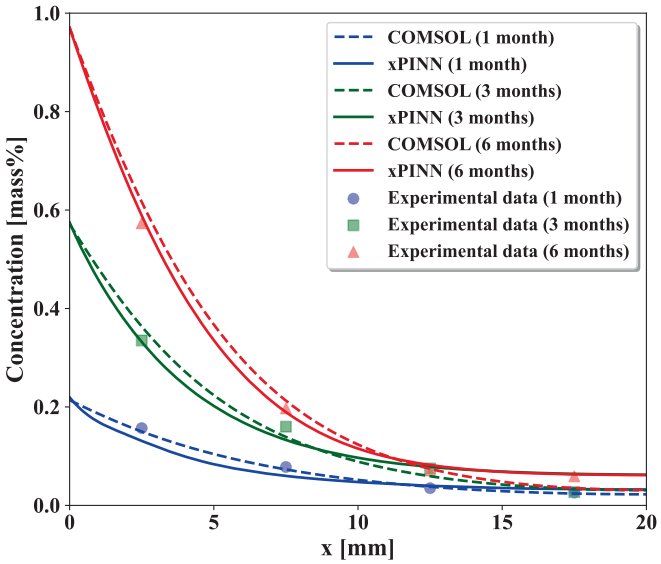

Fig. 31. Test results and COMSOL output, and comparison with the xPINN results.

Table 5
Error indicators for xPINN and COMSOL results vs. test site (Group C).

Exposure months	RMSE		MAE		R^2	
	COMSOL	xPINN	COMSOL	xPINN	COMSOL	xPINN
1 month	4.664e-03	1.644e-02	4.250e-03	1.400e-02	0.991	0.899
3 months	1.984e-02	2.308e-02	1.800e-02	1.761e-02	0.971	0.961
6 months	2.638e-02	1.054e-02	2.200e-02	9.572e-03	0.983	0.997

reproduces the COMSOL predictions; based on this, the DD-PINN, which incorporates the experimental data, further improves the fitting accuracy of the shallow concentration gradient, which is superior to that of the purely physical model.

(2) **Accuracy and robustness of diffusion parameter inversion:** driven by sufficient data, DD-PINN is able to achieve parameter inversion results with an error of less than 10% at $\leq$ 15% input noise, and an error rate of $\pm$ 5% even when referring to the lower data volume of the actual experimental scenarios (set at 10% input noise).

(3) **Strategy for inversion combining data, physics, and engineering insights**: with this strategy, PINN is not only able to reproduce concentration distributions under known initial/boundary conditions, but also to autonomously learn and accurately estimate (within the limits provided by engineering experience) physical parameters, such as diffusion coefficients in one- or two-parameter inversion problems.

(4) **Modelling of xPINN in cracked concrete with the aid of fidelity data assistance:** by introducing FEM high-fidelity data to provide weak constraints for the crack-substrate interface, weakly-supervised xPINN is able to converge stably and identify the diffusion coefficients accurately in both straight and tortuous cracks, which provides a new method for diffusion studies in complex multi-scale crack systems such as Ultra-High Performance Fiber Reinforced Concrete and 3D Printed Concrete.

(5) **Constructed a research framework for the diffusion of self-healing concrete:** xPINN accurately inverted the diffusion coefficients of fully healed cracks and predicted the diffusion concentration in total agreement with COMSOL; the R^2 of fit increased from 0.899 to 0.997 with the increase of exposure time from 1 to 6 months, which verified the excellent performance in long-term diffusion simulation.

PINN also has a wide range of engineering applications. Based on the positive outcomes of this work, the studies can further be employed in:

(I) Extending xPINN to 3D for coupling multidirectional diffusion and crack networks; Efficiently capturing anisotropic transport features and quantifying chloride intrusion rates under complex boundaries through adaptive sampling and multidomain discretization. In parallel, particular attention should be paid to mitigating common PINN issues such as spectral bias and stiffness, to ensure stable training and reliable approximation in these more complex settings.

(II) Instead of relying solely on diffusion, future models should incorporate the combined effects of diffusion, electromigration and convection within a Nernst–Planck equation system. Building on this formulation, the proposed PINN framework can be employed both for forward simulations and for inverse analysis based on experimental measurements. This direction is expected to play an important role in AI-assisted experimental interpretation and durability assessment of reinforced concrete structures.

CRediT authorship contribution statement

Zhewen Huang: Writing – review & editing, Writing – original draft, Visualization, Software, Methodology, Investigation, Funding acquisition, Formal analysis, Conceptualization. **Senlin Xie:** Writing – review & editing, Writing – original draft, Visualization, Software, Methodology, Formal analysis, Conceptualization. **Kasyapa Sriram Kompella:** Writing – original draft, Visualization, Formal analysis. **Estefanía Cuenca:** Writing – review & editing, Supervision, Methodology, Investigation, Data curation, Conceptualization. **Stefano Mariani:** Writing – review & editing, Supervision, Methodology, Formal analysis. **Liberato Ferrara:** Writing – review & editing, Supervision, Project administration, Methodology, Funding acquisition, Formal analysis, Conceptualization.

Declaration of competing interest

The authors declare that they have no known competing financial interests or personal relationships that could have appeared to influence the work reported in this paper.

Acknowledgements

The research activity reported in this paper has been performed as a follow-up to the ReSHEALience project which has received funding from the European Union's Horizon 2020 Research and Innovation Program under grant agreement No 760824. The first author and second author thank the China Scholarship Council (CSC) for financial support during their PhD studies in Structural Geotechnical and Earthquake Engineering at Politecnico di Milano. The last author also acknowledges the support of the MUSA – Multilayered Urban Sustainability Action - project, funded by the European Union – NextGenerationEU, under the National Recovery and Resilience Plan (NRRP) Mission 4 Component 2 Investment Line 1.5: Strengthening of research structures and creation of R&D "innovation ecosystems", set up of "territorial leaders in R&D".

Appendix A. . Pseudo-code of the PINN model for chloride diffusion in concrete

Below is the pseudo-code of the PINN model used to solve the forward / inverse problem in one dimension of chloride diffusion corresponding to that shown in Figs. 3 & 4) is as follows:

Algorithm Structure: Unified PINN for Forward / Inverse Problems
Step 1: Data preparationSampling data points $(\boldsymbol{x}_f, \boldsymbol{t}_f)$ for the PDE interior, $(\boldsymbol{x}_{ic}, \boldsymbol{t}_{ic})$ for I.C., $(\boldsymbol{x}_{bc}, \boldsymbol{t}_{bc})$ for B.C.Load measurement data $(\boldsymbol{x}_{dd}, \boldsymbol{t}_{dd})$ (optional for forward as constraints; required for inverse) and normalize all inputs.Step 2: PINN Model DefinitionBuild a neural network with several hidden layers (e.g., tanh activation).If model used for inverse problem-solving, represent the unknown diffusion coefficient ($\boldsymbol{\beta}$) as a trainable parameter, given an initial value for searching.Step 3: Loss function definitionDefine a loss combining function $\mathscr{L}$ that includes: • $\mathscr{L}_{PDE}$: PDE residual computed via automatic differentiation ▪ (For forward, $\boldsymbol{\beta}$ is known and given; for inverse, $\boldsymbol{\beta}$ is trainable.) • $\mathscr{L}_{B.C.}$ & $\mathscr{L}_{I.C.}$: Constraints for initial and boundary conditions • $\mathscr{L}_{DD}$: Data-driven component (included only if measurement data present) Step 4: Training neural networkTraining with Adam; monitor training & validation losses and PDE residual.Step 5: Output & Estimation • Feed new inputs $(\boldsymbol{x}, \boldsymbol{t})$ into the trained PINN to obtain predictions for the target quantity. • If model used for inverse problem-solving, extract the identified diffusion coefficient $\boldsymbol{\beta}$ from the trained model.

The following pseudocode represents the two-dimensional xPINN model, comprising both the Con-PINN and Cr-PINN networks, corresponding to the operational strategy outlined in Section 4.3.1:

Algorithm Structure: Unified xPINN for Forward / Inverse Problems
Step 1: Data preparationSampling data points $\left(\boldsymbol{x}_f, \boldsymbol{y}_f, \boldsymbol{t}_f\right)$ for the PDE interior, $(\boldsymbol{x}_{ic}, \boldsymbol{y}_{ic}, \boldsymbol{t}_{ic})$ for I.C., $(\boldsymbol{x}_{bc}, \boldsymbol{y}_{bc}, \boldsymbol{t}_{bc})$ for B.C in concrete region and crack region, separately.Load measurement data $(\boldsymbol{x}_{dd}, \boldsymbol{y}_{dd}, \boldsymbol{t}_{dd})$ (optional for forward as constraints; required for inverse) and normalize all inputs.Step 2: PINN Model DefinitionBuild two neural networks (Con-PINN & Cr-PINN) with several hidden layers, independently (e.g., tanh activation).If model used for inverse problem-solving, represent the unknown diffusion coefficient ($\boldsymbol{\beta}$) as a trainable parameter, given an initial value for searching.Step 3: Loss function definitionDefine a loss combining function $\mathscr{L}$ that includes: • $\mathscr{L}_{PDE}$: PDE residual computed via automatic differentiation ▪ (For forward, $\boldsymbol{\beta}$ is known and given; for inverse, $\boldsymbol{\beta}$ is trainable.) • $\mathscr{L}_{B.C.}$ & $\mathscr{L}_{I.C.}$: Constraints for initial and boundary conditions, excluding interface line • $\mathscr{L}_{DD}$: Data-driven component extracts data from along or near the interface line (as a constraint assisting xPINN convergence) • $\mathscr{L}_{int}$: Constraints at interface composited from concentration consistency and flux consistency. Step 4: Training neural networksTraining Con-PINN & Cr-PINN with Adam, separately; only monitor training & validation losses from B.C. & I.C. and PDEJoint training Con-PINN & Cr-PINN as xPINN with Adam; monitor training & validation losses from every itemsStep 5: Output & Estimation • Feed new inputs $(\boldsymbol{x}, \boldsymbol{y}, \boldsymbol{t})$ into the trained PINN to obtain predictions for the target quantity. • If model used for inverse problem-solving, extract the identified diffusion coefficient $\boldsymbol{\beta}$ from the trained model.

Note: All numerical experiments were performed on a desktop workstation equipped with an Intel Core i7-14700F CPU, an NVIDIA GeForce RTX 4060 Ti GPU and 32 GB of RAM. The PINN models were implemented in Python 3.7.0, using CUDA 11.5 and cuDNN 8.3.2. and the networks were trained with PyTorch 1.12.1 and Keras 2.7.0.

Appendix B. . The loss and prediction of Non-Supervised xPINN

Taking the case of concrete with curved crack as an example, the differences between supervised and unsupervised xPINN in terms of loss and simulation prediction results are illustrated in Figs. 32 & 33.

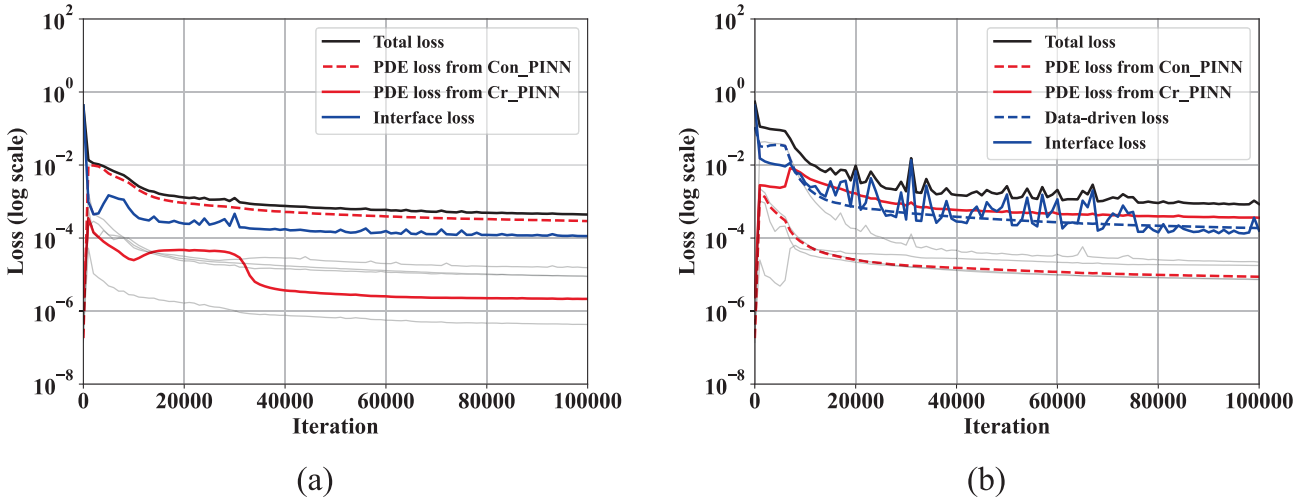

Fig.32. The training loss of (a) non-supervised-PINN and (b) weakly-supervised −PINN.

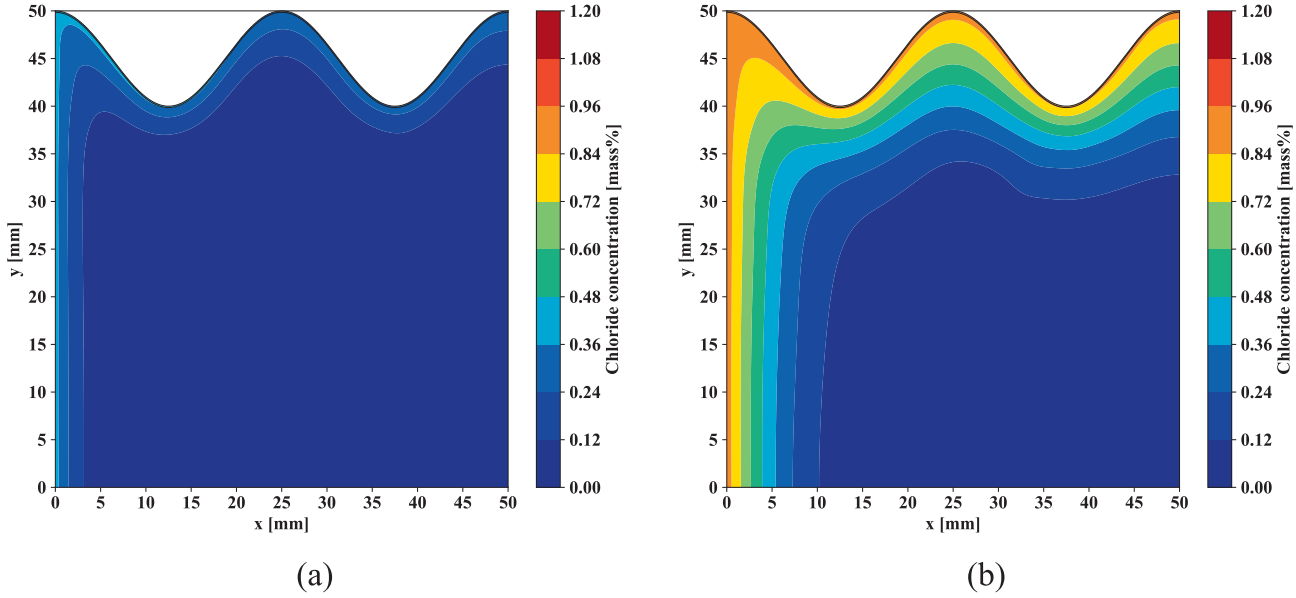

Fig.33. Chloride concentration contour of non-supervised-xPINN after (a)2 months and (b) 8 months exposure.

Appendix C. . Design and derivation of diffusion coefficients for crack phase affected by self-healing phenomena

The relationship between the effective diffusion coefficient in the crack and the crack width has been derived from the experimental results of Djerbi et al [55]. Although the self-healing phenomenon continuously closes the crack space and the crack width decreases, the chemical properties and geometry of the healing products do not remain exactly the same as those of the cement particles. Therefore, it is not possible to adopt the experimental conclusions of Djerbi et al. to describe the dynamics of the diffusion coefficient inside the cracks, which can be referred to the law in Eq. (28) only after cracking or before the beginning of exposure. Considering the diffusion coefficient is linked to the extent of crack healing, a self-healing kinetic model [8,52] must be introduced to quantify the degree of crack closure. The mathematical expression of this model is provided as:

$$ICC = 1 - e^{-S \bullet t}$$

in which ICC is the index of crack closure. When this value is equal to one, it represents the crack completely closed. S is self-healing coefficient from data fitting. Note that this kinetic model is summarized from experimental sample healing stimulated by crystalline admixtures (CA) in mix design [52]. In this study, S is equal to 1 and this model is only from surface area observation. In order to apply this model on design of chloride diffusion coefficient, the assumption of uniformly growing and sealing the crack space by healing products. Therefore, the quantified healing process of surface could be considered as sealing process of entire space in crack.

If it is assumed that the diffusion coefficient is linearly related to the degree of crack closure, the diffusion coefficient of a crack over time can be designed as:

$$D_{cr,de}(t) = D_{cr,o} - \left(D_{cr,o} - D_{CA}\right) \bullet \left(1 - e^{-S \bullet t}\right)$$

where $D_{cr,o}$ is the diffusion coefficient of crack before exposure, and it refers to Eq. (28). D_{CA} is the diffusion coefficient of fully healed crack, which is seen as a constant and could be obtained from PINN inverse study.

Appendix D. . Experimental data summarized from Cuenca et al [48]

Data from	Depth [mm]	Chloride concentration [%]	
		A/B	C
Cracked concrete after 1 month of exposure	2.5	0.143	0.157
	7.5	0.050	0.078
	12.5	0.038	0.035
	17.5	0.035	0.026
Cracked concrete after 3 months of exposure	2.5	0.263	0.335
	7.5	0.058	0.160
	12.5	0.047	0.075
	17.5	0.044	0.027
Cracked concrete after 6 months of exposure	2.5	0.410	0.573
	7.5	0.071	0.197
	12.5	0.060	0.071
	17.5	0.053	0.059

Note: While the weakly-supervised xPINN method is shown to be effective in solving the 2D problem as discussed in section 4.3, a better prediction of the apparent chloride diffusion coefficient of fully healed crack can be made by improving the experimental method elaborated in Cuenca et al. [48], to capture the chloride concentration and thus the diffusion coefficient closer to the healed crack surface than the 5–10 mm presented in literature.

References

[1] Soave F, Ferrara L. A durability- based design approach for structural applications with advanced cement-based materials. Case Stud Constr Mater 2025;22:e04294. https://doi.org/10.1016/j.cscm.2025.e04294.

[2] Al-Obaidi S, Davolio M, Monte FL, Costanzi F, Luchini M, Bamonte P, et al. Structural validation of geothermal water basins constructed with durability enhanced ultra high performance fiber reinforced concrete (ultra high Durability Concrete). Case Stud Constr Mater 2022;17:e01202. https://doi.org/10.1016/j.cscm.2022.e01202.

[3] Ehlen MA, Thomas MD, Bentz EC. Life-365 Service Life Prediction Model™ Version 2.0. Concr Int 2009;31.

[4] fib Bulletins: fib Model Code for Concrete Structures (2020), (n.d.). https://fib-international.org/publications/fib-bulletins/fib-model-code-2020-detail.html (accessed March 18, 2025).

[5] Document BE95-1347/R17 2000.

[6] Luping T. Engineering expression of the ClinConc model for prediction of free and total chloride ingress in submerged marine concrete. Cem Concr Res 2008;38:1092–7. https://doi.org/10.1016/j.cemconres.2008.03.008.

[7] Peng J, Hu S, Zhang J, Cai CS, Li L. Influence of cracks on chloride diffusivity in concrete: a five-phase mesoscale model approach. Constr Build Mater 2019;197:587–96. https://doi.org/10.1016/j.conbuildmat.2018.11.208.

[8] Z. Huang, E. Cuenca, L. Ferrara, Modelling the Effects of Crystalline-Stimulated Self-healing on Chloride Transportation into Cracked Concrete, in: L. Ferrara, G. Muciaccia, D. Di Summa (Eds.), Proceedings of the RILEM Spring Convention and Conference 2024, Springer Nature Switzerland, Cham, 2025: pp. 91–101. https://doi.org/10.1007/978-3-031-70281-5_11.

[9] Cibelli A, Pathirage M, Cusatis G, Ferrara L, Di Luzio G. A discrete numerical model for the effects of crack healing on the behaviour of ordinary plain concrete: Implementation, calibration, and validation. Eng Fract Mech 2022;263:108266. https://doi.org/10.1016/j.engfracmech.2022.108266.

[10] Cibelli A, Ferrara L, Di Luzio G. Multiscale and multiphysics discrete model of self-healing of matrix and interfacial cracks in fibre reinforced cementitious composites: Formulation, implementation and preliminary results. Cem Concr Compos 2024;148:105465. https://doi.org/10.1016/j.cemconcomp.2024.105465.

[11] Zhang Y, Yu L, Yang L, Hu Z, Liu Y. Data-driven framework for predicting rate of penetration in deepwater granitic formations: a marine engineering geology perspective with comprehensive model interpretability. Eng Geol 2025;351:108039. https://doi.org/10.1016/j.enggeo.2025.108039.

[12] Xie S-L, Hu A, Wang M, Xiao Z-R, Li T, Wang C. 1DCNN-based prediction methods for subsequent settlement of subgrade with limited monitoring data. Eur J Environ Civ Eng 2025;29:759–84. https://doi.org/10.1080/19648189.2024.2416441.

[13] Hu A-F, Xie S-L, Li T, Xiao Z-R, Chen Y, Chen Y-Y. Soil parameter inversion modeling using deep learning algorithms and its application to settlement prediction: a comparative study. Acta Geotech 2023;18:5597–618. https://doi.org/10.1007/s11440-023-01935-z.

[14] Zhang Y, Yang L, Fang H, Ma Y, Ning B. Assessment for burst failure of subsea production pipeline systems based on machine learning. Ocean Eng 2024;304:117873. https://doi.org/10.1016/j.oceaneng.2024.117873.

[15] Fernández De La Mata F, Gijón A, Molina-Solana M, Gómez-Romero J. Physics-informed neural networks for data-driven simulation: Advantages, limitations, and opportunities. Physica A 2023;610:128415. https://doi.org/10.1016/j.physa.2022.128415.

[16] Raissi M, Perdikaris P, Karniadakis GE. Physics-informed neural networks: a deep learning framework for solving forward and inverse problems involving nonlinear partial differential equations. J Comput Phys 2019;378:686–707. https://doi.org/10.1016/j.jcp.2018.10.045.

[17] Xie S, Hu A, Xiao Z, Mariani S, G.. Della Vecchia, PINN-based approach to the consolidation analysis of visco-elastic soft soil around twin tunnels. Tunnelling and Underground Space Technology 153 2024:105981. https://doi.org/10.1016/j.tust.2024.105981.

[18] Yu X, Hu T, Khodadadi N, Liu Q, Nanni A. Modeling chloride ion diffusion in recycled aggregate concrete: a fuzzy neural network approach integrating material and environmental factors. Structures 2025;73:108372. https://doi.org/10.1016/j.istruc.2025.108372.

[19] Huang Z, Cuenca E, Ferrara L. Optimized data-driven method to study the self-healing and durability of ultra-high performance concrete. Eng Appl Artif Intel 2025;143:110043. https://doi.org/10.1016/j.engappai.2025.110043.

[20] Xi B, Huang Z, Al-Obaidi S, Ferrara L. Predicting ultra high-performance concrete self-healing performance using hybrid models based on metaheuristic optimization techniques. Constr Build Mater 2023;381:131261. https://doi.org/10.1016/j.conbuildmat.2023.131261.

[21] Yang S, Kim H, Hong Y, Yee K, Maulik R, Kang N. Data-driven physics-informed neural networks: a digital twin perspective. Comput Methods Appl Mech Eng 2024;428:117075. https://doi.org/10.1016/j.cma.2024.117075.

[22] Zhao BR, Sun DK, Wu H, Qin CJ, Fei QG. Physics-informed neural networks for solving inverse problems in phase field models. Neural Netw 2025;190:107665. https://doi.org/10.1016/j.neunet.2025.107665.

[23] Guo R, Wang J, Yuan Y, Li D, Jin Y, Shan H. Interpretation of dual time-dependent chloride diffusion in concrete based on physical information neural networks. Case Stud Constr Mater 2024;21:e03769. https://doi.org/10.1016/j.cscm.2024.e03769.

[24] Song C, Xiao R, Zhang C, Zhao X, Sun B. Simulation-free reliability analysis with importance sampling-based adaptive training physics-informed neural networks: Method and application to chloride penetration. Reliab Eng Syst Saf 2024;246:110083. https://doi.org/10.1016/j.ress.2024.110083.

[25] Wan Y, Zheng W, Wang Y. Identification of chloride diffusion coefficient in concrete using physics-informed neural networks. Constr Build Mater 2023;393:132049. https://doi.org/10.1016/j.conbuildmat.2023.132049.

[26] Shaban WM, Elbaz K, Zhou A, Shen S-L. Physics-informed deep neural network for modeling the chloride diffusion in concrete. Eng Appl Artif Intel 2023;125:106691. https://doi.org/10.1016/j.engappai.2023.106691.

[27] Wu R, Xia Y, Xia J. Long-term prediction of surface chloride content of marine concrete structures using inverse physics-informed neural networks. Eng Struct 2025;329:119752. https://doi.org/10.1016/j.engstruct.2025.119752.

[28] Söyleyici C, Ünver HÖ. A Physics-Informed Deep Neural Network based beam vibration framework for simulation and parameter identification. Eng Appl Artif Intel 2025;141:109804. https://doi.org/10.1016/j.engappai.2024.109804.

[29] Zhang J, Chiu S-T, Braga-Neto U, Gildin E. Physics-Informed Neural Networks for CO 2 migration modeling in stratified saline aquifers: applications in geological carbon sequestration. Geoenergy Sci Eng 2025;247:213689. https://doi.org/10.1016/j.geoen.2025.213689.

[30] Ameya ADJ, Jagtap D, G.E.K. George Em Karniadakis. Extended Physics-Informed Neural Networks (XPINNs): a Generalized Space-Time Domain Decomposition

based Deep Learning Framework for Nonlinear Partial Differential Equations. CICP 2020;28. https://doi.org/10.4208/cicp.OA-2020-0164.
[31] Jagtap AD, Kharazmi E, Karniadakis GE. Conservative physics-informed neural networks on discrete domains for conservation laws: applications to forward and inverse problems. Comput Methods Appl Mech Eng 2020;365:113028. https://doi.org/10.1016/j.cma.2020.113028.
[32] Ann KY, Ahn JH, Ryou JS. The importance of chloride content at the concrete surface in assessing the time to corrosion of steel in concrete structures. Constr Build Mater 2009;23:239–45. https://doi.org/10.1016/j.conbuildmat.2007.12.014.
[33] Luping T, Nilsson L-O. Chloride diffusivity in high strength concrete at different ages. accessed March 13, 2025 NORDIC CONCRETE RESEARCH PUBLICATION NO 1992;11. https://trid.trb.org/View/376238.
[34] Takewaka K, Mastumoto S. Quality and cover thickness of concrete based on the estimation of chloride penetration in marine environments, special. Publication 1988;109:381–400.
[35] Petcherdchoo A. Time dependent models of apparent diffusion coefficient and surface chloride for chloride transport in fly ash concrete. Constr Build Mater 2013;38:497–507. https://doi.org/10.1016/j.conbuildmat.2012.08.041.
[36] Cai R, Yu M, Hu Y, Yang L, Ma H. Influence of data acquisition and processing on surface chloride concentration of marine concrete. Constr Build Mater 2021;273:121705. https://doi.org/10.1016/j.conbuildmat.2020.121705.
[37] Luping T, Gulikers J. On the mathematics of time-dependent apparent chloride diffusion coefficient in concrete. Cem Concr Res 2007;37:589–95. https://doi.org/10.1016/j.cemconres.2007.01.006.
[38] Boddy A, Bentz E, Thomas MDA, Hooton RD. An overview and sensitivity study of a multimechanistic chloride transport model. Cem Concr Res 1999;29:827–37. https://doi.org/10.1016/S0008-8846(99)00045-9.
[39] Andrade C, J.M. Díez, C. Alonso. Mathematical modeling of a concrete surface "skin effect" on diffusion in chloride contaminated media. Adv Cem Bas Mat 1997;6:39–44.
[40] Stipanovic Oslakovic I, Bjegovic D, Mikulic D. Evaluation of service life design models on concrete structures exposed to marine environment. Mater Struct 2010;43:1397–412. https://doi.org/10.1617/s11527-010-9590-z.
[41] Karlik B, Olgac AV. Performance analysis of various activation functions in generalized MLP architectures of neural networks. International Journal of Artificial Intelligence and Expert Systems 2011;1:111–22.
[42] Shen S-L, Zhang N, Zhou A, Yin Z-Y. Enhancement of neural networks with an alternative activation function tanhLU. Expert Syst Appl 2022;199:117181.
[43] Xie S, Hu A, Mariani S, G.. Della Vecchia, PINN-based approach to the nonlinear large-strain consolidation under time-dependent drainage boundary. Acta Geotech 2025;20:5941–69. https://doi.org/10.1007/s11440-025-02729-1.
[44] Baydin AG, Pearlmutter BA, Radul AA, Siskind JM. Automatic differentiation in machine learning: a survey. J Mach Learn Res 2018;18:1–43.
[45] Luong KA, Wahab MA, Lee JH. Simultaneous imposition of initial and boundary conditions via decoupled physics-informed neural networks for solving initial-boundary value problems. Appl Math Mech-Engl Ed 2025;46:763–80. https://doi.org/10.1007/s10483-025-3240-7.
[46] Qian Y, Zhang Y, Huang Y, Dong S. Physics-informed neural networks for approximating dynamic (hyperbolic) PDEs of second order in time: Error analysis and algorithms. J Comput Phys 2023;495:112527. https://doi.org/10.1016/j.jcp.2023.112527.
[47] Angst U, Elsener B, Larsen CK, Vennesland Ø. Critical chloride content in reinforced concrete—A review. Cem Concr Res 2009;39:1122–38.
[48] Cuenca E, Lo MF, Moro M, Schiona A, Ferrara L. Effects of Autogenous and Stimulated Self-Healing on Durability and Mechanical Performance of UHPFRC: Validation of Tailored Test Method through Multi-Performance Healing-Induced Recovery Indices. Sustainability 2021;13:11386. https://doi.org/10.3390/su132011386.
[49] Thomas MDA, Bamforth PB. Modelling chloride diffusion in concrete effect of fly ash and slag. Cem Concr Res 1999.
[50] Chalee W, Jaturapitakkul C, Chindaprasirt P. Predicting the chloride penetration of fly ash concrete in seawater. Mar Struct 2009;22:341–53. https://doi.org/10.1016/j.marstruc.2008.12.001.
[51] Cappellesso V, Di Summa D, Pourhaji P, Prabhu Kannikachalam N, Dabral K, Ferrara L, et al. A review of the efficiency of self-healing concrete technologies for durable and sustainable concrete under realistic conditions. Int Mater Rev 2023;68:556–603. https://doi.org/10.1080/09506608.2022.2145747.
[52] Huang Z, Cuenca E, Ferrara L. Incorporation of self-healing of UHPC in structural design approaches through healable crack width threshold and kinetics: the case study of H2020 project ReSHEALience database. Dev Built Environ 2024;18:100388. https://doi.org/10.1016/j.dibe.2024.100388.
[53] Hu Z, Jagtap AD, Karniadakis GE, Kawaguchi K. When do Extended Physics-Informed Neural Networks (XPINNs) Improve Generalization. SIAM J Sci Comput 2022;44:A3158–82. https://doi.org/10.1137/21M1447039.
[54] Rezaei S, Harandi A, Moeineddin A, Xu B-X, Reese S. A mixed formulation for physics-informed neural networks as a potential solver for engineering problems in heterogeneous domains: Comparison with finite element method. Comput Methods Appl Mech Eng 2022;401:115616. https://doi.org/10.1016/j.cma.2022.115616.
[55] Djerbi A, Bonnet S, Khelidj A, Baroghel-Bouny V. Influence of traversing crack on chloride diffusion into concrete. Cem Concr Res 2008;38:877–83. https://doi.org/10.1016/j.cemconres.2007.10.007.
[56] Chakraborty S. Transfer learning based multi-fidelity physics informed deep neural network. J Comput Phys 2021;426:109942. https://doi.org/10.1016/j.jcp.2020.109942.
[57] Mitusch SK, Funke SW, Kuchta M. Hybrid FEM-NN models: Combining artificial neural networks with the finite element method. J Comput Phys 2021;446:110651. https://doi.org/10.1016/j.jcp.2021.110651.
[58] Wang Y, Wu L, Wang Y, Li Q, Xiao Z. Prediction model of long-term chloride diffusion into plain concrete considering the effect of the heterogeneity of materials exposed to marine tidal zone. Constr Build Mater 2018;159:297–315. https://doi.org/10.1016/j.conbuildmat.2017.10.083.
[59] Stanish K, Thomas M. The use of bulk diffusion tests to establish time-dependent concrete chloride diffusion coefficients. Cem Concr Res 2003;33:55–62. https://doi.org/10.1016/S0008-8846(02)00925-0.
[60] B. Martín-Pérez, H. Zibara, R.D. Hooton, M.D.A. Thomas. A study of the effect of chloride binding on service life predictions. Cem Concr Res 2000;30:1215–23. https://doi.org/10.1016/S0008-8846(00)00339-2.
[61] Kim J, McCarter WJ, Suryanto B, Nanukuttan S, Basheer PAM, Chrisp TM. Chloride ingress into marine exposed concrete: a comparison of empirical- and physically-based models. Cem Concr Compos 2016;72:133–45. https://doi.org/10.1016/j.cemconcomp.2016.06.002.
[62] Yang LF, Cai R, Yu B. Investigation of computational model for surface chloride concentration of concrete in marine atmosphere zone. Ocean Eng 2017;138:105–11. https://doi.org/10.1016/j.oceaneng.2017.04.024.
[63] Kassir MK, Ghosn M. Chloride-induced corrosion of reinforced concrete bridge decks. Cem Concr Res 2002;32:139–43. https://doi.org/10.1016/S0008-8846(01)00644-5.
[64] Costa A, Appleton J. Chloride penetration into concrete in marine environment—Part I: Main parameters affecting chloride penetration. Mat Struct 1999;32:252–9. https://doi.org/10.1007/BF02479594.
[65] Pack S-W, Jung M-S, Song H-W, Kim S-H, Ann KY. Prediction of time dependent chloride transport in concrete structures exposed to a marine environment. Cem Concr Res 2010.
[66] Song H-W, Lee C-H, Ann KY. Factors influencing chloride transport in concrete structures exposed to marine environments. Cem Concr Compos 2008;30:113–21. https://doi.org/10.1016/j.cemconcomp.2007.09.005.